공학석사 학위논문

# Characteristics of Helium Atmospheric Pressure Plasma Bullet Propagation

# 헬륨 상압 플라즈마 불렛의 진행 특성

2014 년 2 월

서울대학교 대학원

에너지시스템공학부

김 수 정

# Characteristics of Helium Atmospheric Pressure Plasma Bullet Propagation

# 헬륨 상압 플라즈마 불렛의 진행 특성

지도교수 김 곤 호

이 논문을 공학석사 학위논문으로 제출함
2014 년 2 월

서울대학교 대학원
에너지시스템공학부
김수정

김수정의 공학석사 학위논문을 인준함
2014 년 2 월

위 원 장 황 용 석 (인)

부위원장 김 곤 호 (인)

위 원 조 철 훈 (인)

# Abstract

Helium Atmospheric Pressure Plasma Jets (He-APPJs) are frequently used for bio-medical treatments due to the advantages of easy to use, high production of reactive radicals and low gas temperature. In spite of the efforts of application on bio-medical fields, difficulties for securing the reproducibility among experiments still exist. This is caused by the lack of understanding APPJ plumes in which the discrete bullets are continuously propagating. Spatial distribution of bullet velocity and radical density cause the treatment results of target, which varied with the location in APPJ plume. In this thesis, the bullet propagation mechanisms along the plasma plume are studied.

Because the bullet propagates in ambient gas, the ratio of $N_2/O_2$ and He in plasma plume is an important parameter so the molar fraction ratio of $N_2$ and $O_2$ in ambient gas is controlled in this study. To measure the bullet velocity, Intensified Charge-Coupled Device (ICCD) camera was employed with the exposure time of 50 nsec. Optical Emission Spectroscopy method also introduced to monitor the excited, ionized species and to estimate the electric field in the plasma plume. The effect of ambient gas mixture on bullet propagation was analyzed with the bullet velocity model which was developed

from the cathode-directed streamer. Reactor discharge effect was also considered in field analysis in the plume.

ICCD results show that bullet velocity is distributed along the plasma plume and it can be classified with the three of velocity phases. In the phase 1, the bullet gets out the quartz tube exit and the Penning ionization of $N_2$ and $O_2$ entrained from the ambient enhances the speed of bullet propagation. In the phase 2, plasma is discharged in reactor quartz tube and the electric field from accumulated charges on quartz drags the bullet propagation, resulting that the acceleration force becomes zero and the bullet velocity is maintained constant during until the reactor discharge is off. In the phase 3, the excessive $O_2$ entrain into He causes the electron loss by attachment to $O_2$ so the discharge becomes weaker and the bullet velocity linearly decreases with time.

The analysis reveals that the reactor discharge should be considered to understand the bullet behavior in space. In addition, it can be inferred that the position of bio-medical targets is important for the proper purpose of that treatment because it changes the gas flow and molar fraction in plasma plume which have crucial roles in bullet propagation and the spatial distribution of charges and radicals.

**Keywords:** Helium atmospheric pressure plasma jets, bullet velocity, velocity distribution, Penning ionization

# Contents

# List of Figures

# List of Tables

# Chapter 1

# Introduction

## 1.1 Helium Atmospheric Pressure Plasma Jets (He-APPJs) and Bullet Formation

Atmospheric Pressure Plasma Jets (APPJs) are sub-mm size plasma source, operating in room gas temperature and high radical density [1]. Since the plasma produced excited species, charges, and radicals are ejected from reactor to treated substrate, it is useful in need of remote source. In these days, APPJ sources are used in sterilization of bacteria, cancer cell treatment, polymer deposition or etch and beauty treatment like whitening of teeth [2, 3], and so on. However one-to-one comparison of experiments is difficult because of the different reactor structures and driving conditions (applied voltage

amplitude, frequency, shape, ambient and discharge gases etc.). As a result, reproducibility cannot be deduced even though the similar or identical APPJs are used.

General types of APPJ discharge reactor are shown in Figure 1.1, similar to Dielectric Barrier Discharge (DBD) sources ( [4]). Dielectric tube guides the discharge gas and a pair of electrodes is located around the tube or one of the electrodes is at center. The electric field strength inside the reactor is determined by electrode location so the breakdown voltage and discharge current are varied with the separation of electrodes. Since the discharge gas like Helium and Argon are chosen and they are filled in a discharge tube, the discharge in reactor discharge can be considered as pure inert gas discharge. Then the excited and ionized species are ejected from the dielectric tube and initiates bullet propagation in ambient air, forming a plasma plume. In contrast to the discharge in reactor, inert gas is mixed with ambient air and the gas composition of the spot where the bullet is located is important since the discharge in a bullet is necessary to propagate.

In spite of weak or no external electric field in ambient air region, the plasma plume extends to several cm long. When plasma plume is captured by Intensified Charge-Coupled Device (ICCD) camera with very short exposure time about 10~50 nsec, it is found that the plasma plume is not a

continuous form but consist of discrete ‘bullet’ and it moves with several ~km/sec, which is 1000 times faster than neutral gas flow of several ~m/sec [5]. The spherical region emitting light is called as a bullet because it looks like a one ejected from a gun. This bullet property is similar to the streamer head where the ionization and excitation processes are actively proceeded with high electric field generated by space charges in streamer head. This is the reason why the plasma plume can be maintained in spite of the absence of external electric field. The electric field at bullet head and the metastables are easily ionized in the inert–air mixture. This discharge drives bullet itself in ambient air

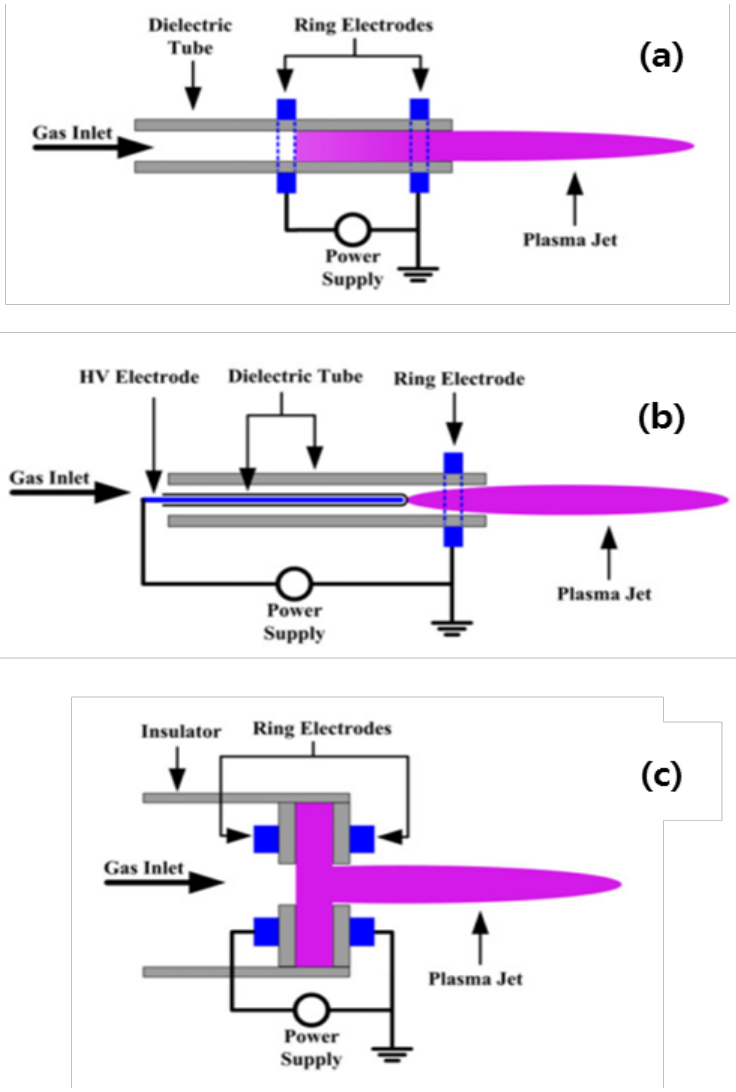


Figure 1.1 Schematic diagrams of DBD-like APPJ reactor structures

: A pair of electrode rings around the dielectric tube (a), powered pin at center and a grounded ring (b), and a pair of electrode rings faced with dielectric disk inside the insulator (c), referred in [4]

## 1.2 Necessity of Bullet Propagation Velocity and Mechanisms in space for the treatments

When the bullet propagates in ambient air, charged particles which consist of electron, positive and negative ions and radicals are generated along plasma plume. Charges are concentrated in bullet head region, due to the necessity of high electric field for the e−n collision ionization and the radicals more spread out in space along the neutral gas flow. These plasma products play an important role in bio−medical applications such as non−thermal sterilization, using highly reactive radicals and the electrostatic disruption of membrane by electrons [6].

To analyze the interaction between plasma products and bio substrates, radical and charge fluxes should be known. These fluxes are function of particle density and its velocity,

$$\Gamma_i = n_i(z)v_i(z) \qquad (1.1)$$

where $i$ is electron, ion and radicals, $n_i(z)$ is particle density and $v_i(z)$ is its velocity at $z$ position. Since charges and radicals are produced through e−n collision processes and the reaction rates are function of reduced electric field at bullet

head, also the bullet velocity, particle densities can be estimated from the bullet propagation velocity with particle balance equations. Consequently the charge and radical density fluxes are explained with bullet propagation velocity. Understanding the bullet propagation velocity and its mechanisms in ambient air are important in order to provide guidelines for optimized operating conditions in the treatment.

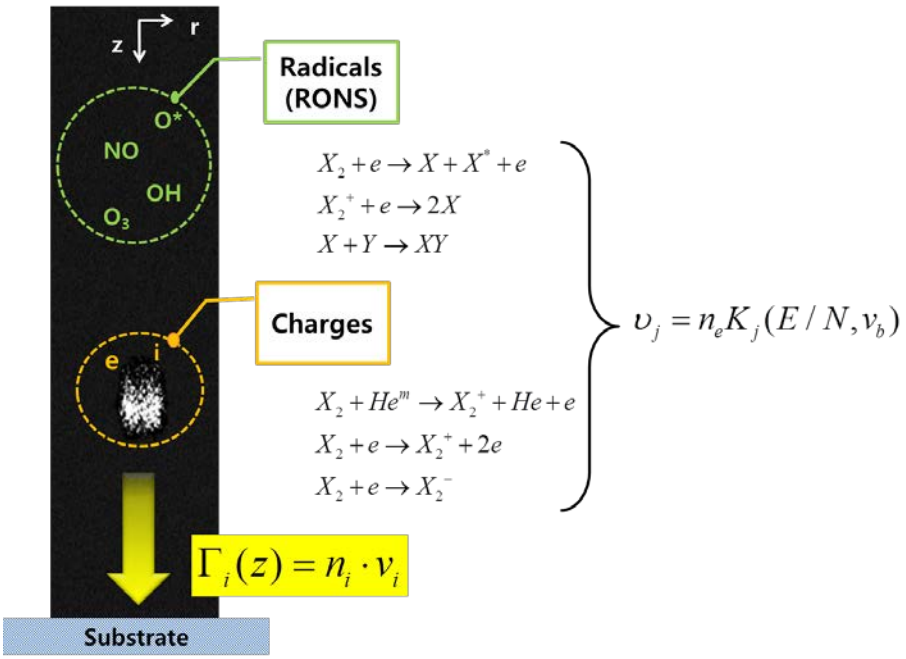


Figure 1.2 Bullet velocity for charge and radical fluxes on treated substrate

: Reactions for charge and radical generations in space. $\upsilon_j$ is reaction frequency of j such as ionization, dissociation, excitation and attachment.

## 1.3 Previous Studies for Bullet Propagation Mechanisms

E Karakas et. al. [6, 7] found that the bullet propagation velocities have spatial distribution and it consists of three phases: the launching, the propagation and the ending phase. The three phases of bullet velocity are cannot fully explained simply because of the discontinuous change of phases. In the launching phase, bullet velocity increases sharply. When the bullet enters into the propagation phase, the acceleration abruptly changes and the bullet propagates several centimeters with constant velocity. In the ending phase, bullet velocity starts to be decelerated and finally disappeared. In [8, 9], bullet formation process and its propagation mechanisms based on the cathode directed streamer are suggested. At first, electrons start avalanche reaction inside the dielectric chamber when the applied voltage increases and exited ions form space electric field which enhances the photoionization, which generate photo-electrons and these electrons accelerate to the head of bullet. By repeating these processes, the bullet propagates in ambient air. When the applied pulse voltage off, the secondary discharge is ignited due to accumulated charges on the dielectric surface. As a result of this discharge, opposite

electric field to the bullet head one is formed so photo-electron cannot maintain avalanche process and bullet becomes very weak. These are the two main discharge mechanisms in the bullet propagation in ambient gas: one is the electron-neutral collision ionization at bullet head during the photo-electron avalanche and another one is external electric field which is opposite to the bullet propagation due to reactor discharge. In addition to these two mechanisms for analysis of bullet propagation, the reactions between $He^m$ and the ambient air molecules should be considered. He has several metastable states that the energy levels are higher than threshold energy of ambient air gas, $N_2$, $O_2$ and $H_2O$ so that the ambient molecules can be ionized by $He^m$, which is called Penning ionization. Unlike that e-n collision ionization rate depends on the electric field, the reaction rate of Penning ionization is independent on electric field and have constant value because it is a reaction between neutrals. In extreme case that there is no electron for ionizing the gases but sufficient $He^m$ density, breakdown can be occurred by Penning ionization. Addition to the e-n collision ionization, Penning reactions increase the electron density then electric field is increased at the head. Increment of electric field at head enhances avalanches and also He excitations so that the electron density again increases and electric field, too. The penning ionization by $He^m$ is an important

mechanism for bullet propagation so here the density ratio between ambient gas and $He^m$ should be considered. In a plasma plume, ambient gas like $N_2$ and $O_2$ are radially entrained in plasma plume and He species diffuses out. The Penning reactions between the $He^m$ and those entrained air molecules are active at radial edge of bullet, resulting that $N_2^+$ ion density distribution along the radial position has peak at the edge [10]. However $N_2$ and $O_2$, have different gas property as the positive and negative gas respectively so that they work on bullet propagation differently. $O_2$ forms negative ions easily so reduces the electron density as well as provides electrons through penning ionization reaction. Also, photons from excited $N_2$ species below 200 nm ionize the $O_2$, producing the photo-electrons, which can act as seed electrons in front of bullet head. In pure $N_2$ condition, photo-electrons are generated far less because of the quenching reactions by itself but there is no loss by attachment. In these reasons, bullet velocity is a function of the gas molar fraction ratios between $N_2$, $O_2$ and He. Thus it is necessary to find out the relation between them to understand the bullet propagation mechanisms. Even though E karakas et. al. suggested the mechanisms with three phases, it is not sufficient to explain why the bullet can be accelerated with some increment rate at launching phase, the velocity phase is suddenly changed at propagation phase and the bullet has

km/sec order of velocities. In following chapters, changes of spatial distribution of bullet velocity are deduced by controlling the ambient $N_2$, $O_2$ gas fraction and the mechanisms of bullet propagation in each phase based on the experimental data are explained with analytic model for bullet propagation velocity.

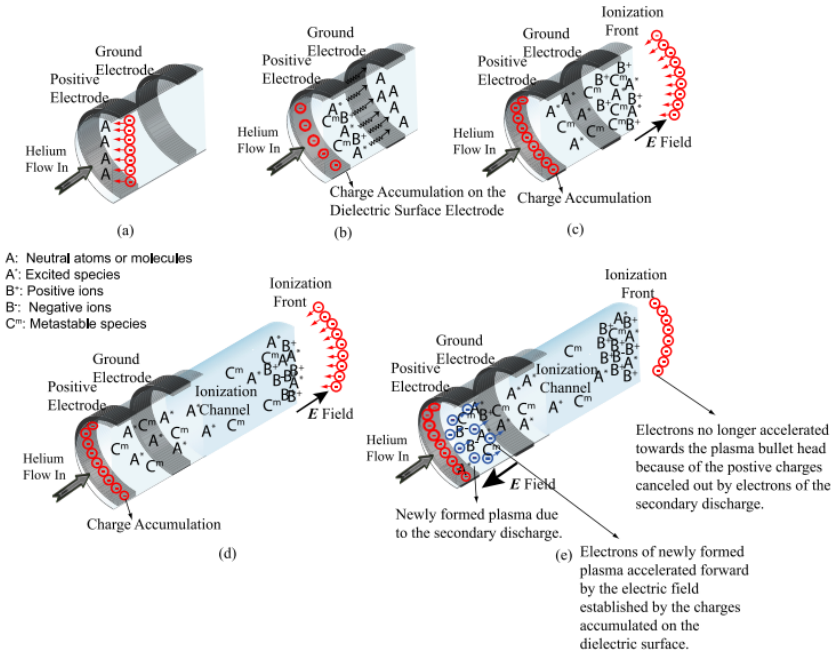


Figure 1.3 Plasma bullet formation and propagation process suggested in [5]

# Chapter 2

# Experimental Setup

## 2.1 Ambient Gas Controllable APPJ and the Diagnostic System

To control the ambient gas condition, the APPJ is discharged in sealed chamber as shown in the Figure 2.1. APPJ reactor body made by Teflon is connected to the He gas and quartz tube is fitted in this body. Outer and inner diameters of quartz tube are 5 mm and 2 mm respectively. The Helium gas flow rate is fixed in 1 lpm (liter per minute) using mass flow controller (Celerity, TN2911V-4S) in all experiment for the laminar flow in and out of quartz tube. The chamber is pumped out to 50 mTorr at which the impurity is below 0.001% and refilled by $N_2$ and $O_2$ gases. The total flow rate of $N_2$ and $O_2$ is

set to 5 lpm and the ratio is changed as shown in Table 1. Details of the reactor design can be referred to the Figure 2.2. A pair of copper electrodes, wrapped around the quartz tube, consists of the bottom and top electrode. Bottom one is connected to high voltage output of voltage amplifier (Trek, 20/20C) for amplifying 2000 times and the upper one is connected to the dummy capacitor(2000 $\mu$F) for measuring the accumulated charge inside the quartz tube. Voltage shape is generated from function generator (Agilent 33220A, 20 MHz) with 6.3 kVpp and 22 kHz sine wave. Distance between the electrodes is 15mm and bottom power electrode is located at 5mm from the quartz exit. Synchronized signal produced from function generator is input to Intensified Charge-Coupled Device (ICCD) controller. This synchronized signal is a reference to take the bullet image by using ICCD (Princeton Instrument Acton, PI-MAX2: 1024i) and camera lens (Nikon, AF Nikkor 85mm f/1.8D)) in image mode. Details of measurement method are explained in the next chapter. From the ICCD equipped to the monochromater (Princeton Instrument Acton, SP 2500i), the optical emission from the plasma plume can be detected by using optical fiber. Two lenses are used in front of the fiber to focus the precise position at plume with 100 μm resolution.

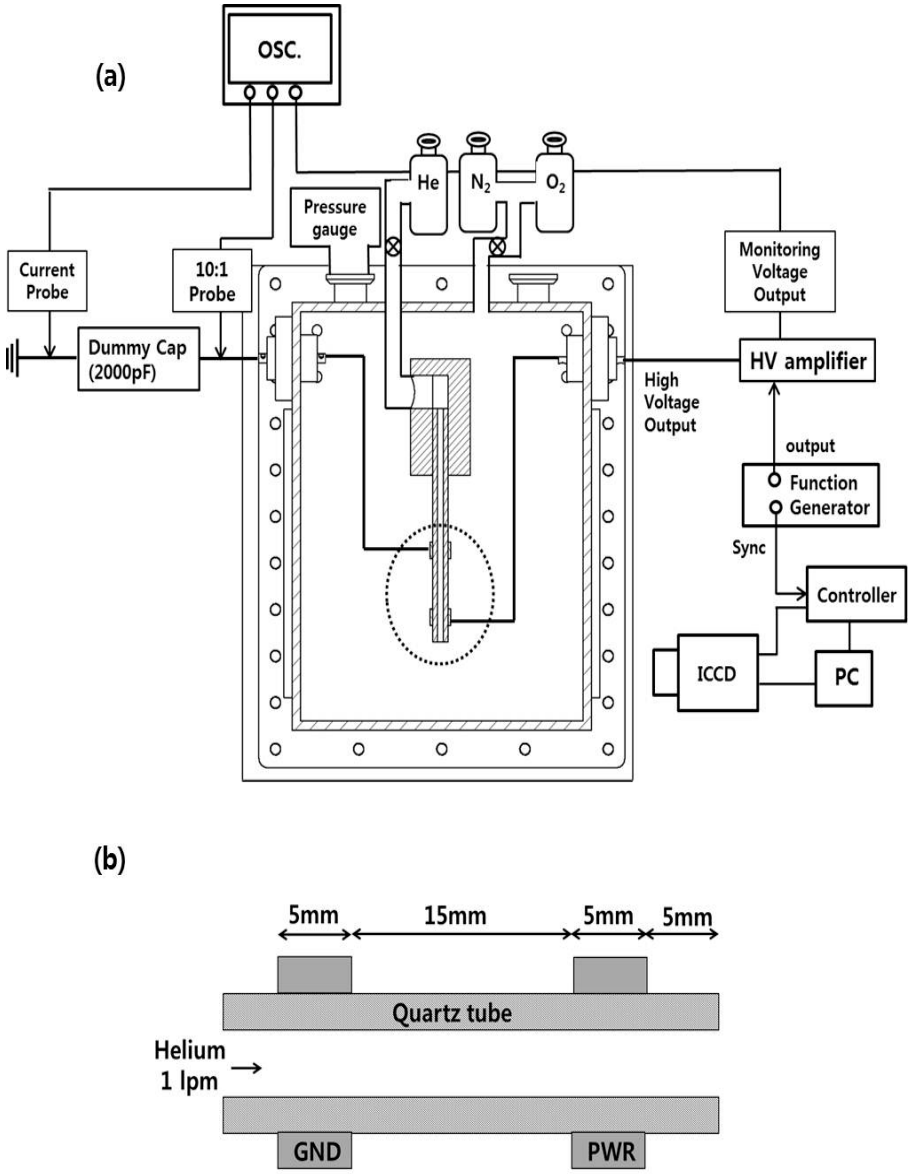


Figure 2.1 Schematic diagram of experimental setup

: APPJ in sealed chamber with diagnostic system (a) and the electrode in dashed circle is magnified in (b)

Table 1 conditions of $N_2/O_2$ mass flow rate for controlled ambient mixture

| $O_2$ fraction | 0 | 0.1 | 0.2 | 0.8 | 1 |
|---|---|---|---|---|---|
| $N_2$ (lpm) | 5 | 4.5 | 4 | 1 | 0 |
| $O_2$ (lpm) | 0 | 0.5 | 1 | 4 | 5 |

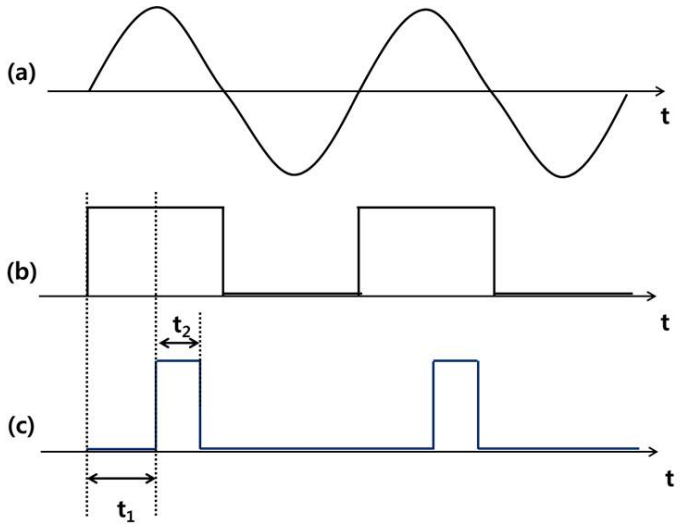


Figure 2.2 Electrical signals of (a) applied voltage, (b) synchronized voltage from function generator and (c) ICCD camera operation

: $t_1$ is the delay time and $t_2$ is the gate width time during which ICCD camera captures the images

## 2.2 Bullet Velocity Measurement by ICCD Images

The synchronized signal from the function generator is used for the reference to ICCD operation. Applied voltage, synchronized signal and ICCD operation time are shown in Figure 2.2. Delay time which means the interval time between sync signal on and the moment of image capturing by ICCD can be set in PC because it is connected with ICCD controller. Proper exposure time is required to measure the bullet position because the intensity from bullet can damage the ICCD with too long exposure time and on the contrary, too low intensity to identify the bullet position. In this experiment, step of delay and exposure time was set to 100 nsec and 50 nsec respectively: Interval of each image is 100nsec and exposure is 50 nsec. The series of bullet image is shown in Figure 2.3. Dashed line is quartz tube exit. The bullet intensity is digitalized at each pixel and maximum value can be found by Matlab code. From the pixels which have maximum bullet intensity the bullet position and velocity can be calculated because instant bullet velocity is $v_b(t) = \frac{z(t+dt) - z(t)}{dt}$. Then bullet position – time, bullet velocity – time and bullet velocity – position graphs can be obtained.

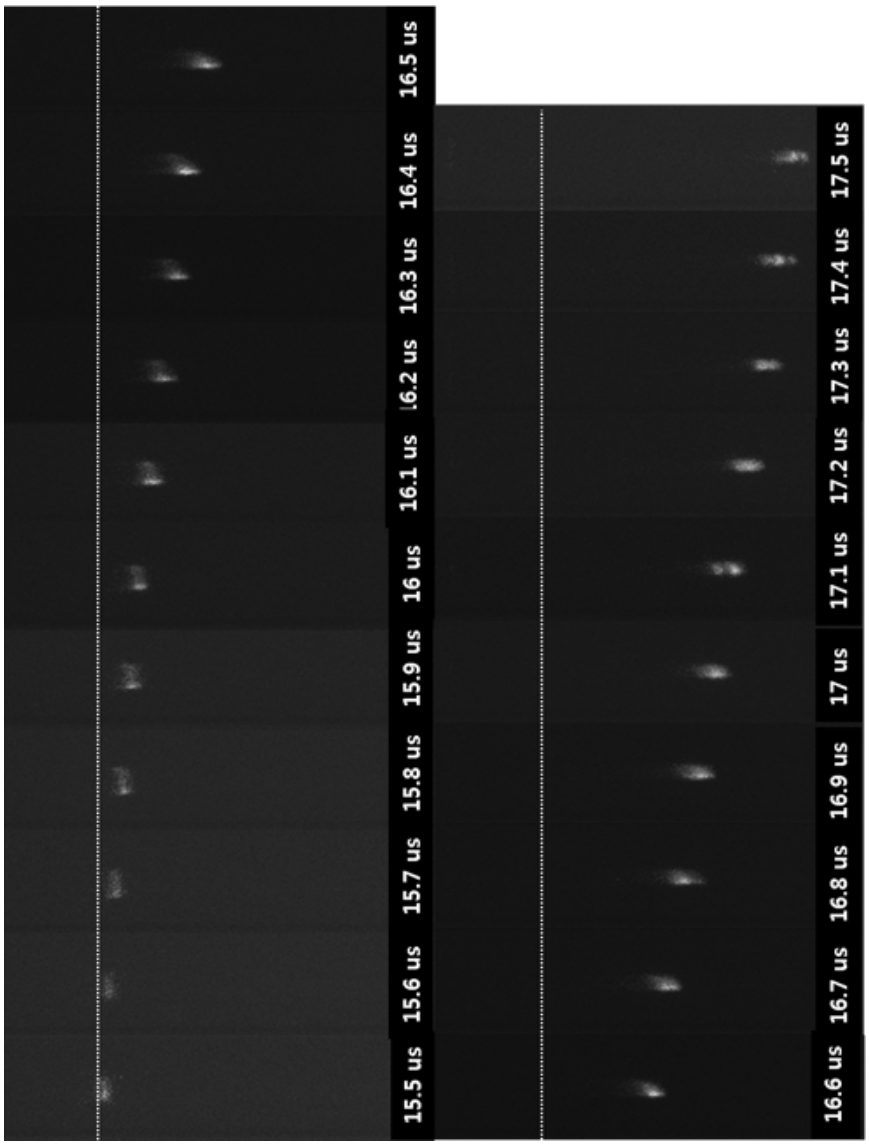


Figure 2.3 Series of bullet images
: Exposure and interval time is 50 nsec and 100 nsec.

# Chapter 3

# Experimental Results

## 3.1 Bullet Velocity and V-I in Ambient air and $N_2/O_2$ Mixtures

Bullet position and velocity are measured in ambient air and $N_2/O_2$ gas mixture by using ICCD images introduced in chapter 2.2. Figure 3.1 is the results of bullet velocity in ambient air condition. Position 0 mm means the quartz tube exit. There are three phases of bullet propagation velocity along the plasma plume which is similar to the results in [6]. Phase 1 (A-B) is acceleration, phase 2 (B-C) is relatively constant velocity and phase 3 (C-D) is deceleration. In the quartz tube, bullet velocity oscillates approximately 2 km/sec. When the bullet

gets out the quartz tube exit, which is correspond to A position in Figure 3.1, it is accelerated up to 13 km/sec. Bullet propagation phase suddenly changes at B and maintain its velocity to be constant. Note that the phase changed not gradually. The drastic change is discussed in chapter 4.3. At C, bullet velocity decreases and its propagation is stopped at D. The full length of plasma plume is about 20 mm.

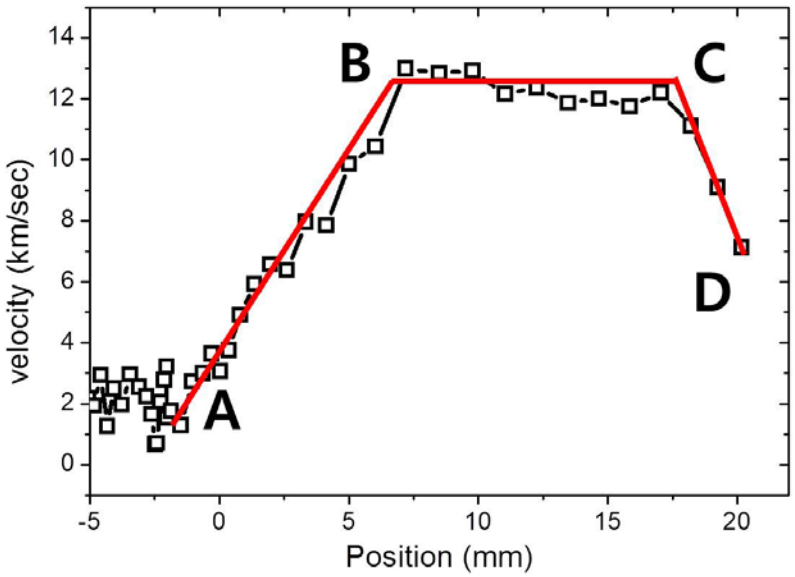


Figure 3.1 Bullet velocity in ambient air condition

In $N_2/O_2$ gas mixture condition, bullet propagation velocities have also three phases as shown in Figure 3.2. $n_{O2}/n_g$ means ratio between $O_2$ molar fraction and total gas mixture. The

length is longer than 20 mm and the maximum velocity is faster than 20 km/sec. Even though $n_{O2}/n_g$ =0.2, which is the simulated condition of dry air, jet length and velocity exceed the value of ambient air condition. This may be caused by the relative humidity which is the ratio of the partial pressure of water vapor in an air−water mixture to the saturated vapor pressure of water. Because the temperature was maintained constant around 20 ℃, the absolute humidity is proportional to the relative one. Relative humidity can be changed from 60 to 80% in summer, the rainy season, and from 20 to 40% in winter, the dry season. The range of humidity during a day can affect the bullet velocity and its stability. $H_2O$ is an electro negative gas for a discharge because it easily forms the negative ion by dissociative electron attachment so it reduces the electron density. In the controlled ambient condition, the percentage of impurities is less than 0.001% and it can be considered that there was no $H_2O$. The difference of overall jet length and velocity between in the normal ambient air and controlled condition may be due to whether $H_2O$ molecules are in or not. In controlled condition, $H_2O$ effects are not considered in this study.

To explain the characteristics and discharge mechanisms for bullet propagation in three regions, it should be analyzed what external parameters affect the acceleration rates in phase

1 (A−B), result sudden change from acceleration to constant velocity in phase 2 (B−C) and vary the start position of phase 3 (C).

The reason of sudden change at B position can be inferred from discharge current in source reactor. In opposite side of bullet propagation, He gas which flows through the electrodes is discharged in reactor for the high applied electric field between electrodes. Its applied voltage and discharge current during the cycle are shown in Figure 3.3. Note that the discharge currents do not mean the bullet current in ambient air because the discharge is not connected to the bullet discharge. However, this current direction is opposite to the direction of bullet propagation. Thus the current peak is observed at positive voltage phase and the displacement current is only in negative phase. The breakdown voltages when the positive currents have peak are almost constant with ambient $N_2/O_2$ mixture ratio even though the current amplitudes are slightly different.

Figure 3.4 shows the discharge current in reactor and bullet velocity in the case of $n_{O2}/n_g$=0.2. Discharge at the edge of power electrode starts at 15.8 $\mu$sec and bullet propagates along the quartz tube. Velocity is about 2.5 km/sec. At 16.6 $\mu$sec, the bullet exit the quartz tube and propagates the ambient mixture gas. Until the bullet propagates outside of the quartz tube about 5 mm from the quartz exit, there is no discharge inside the reactor.

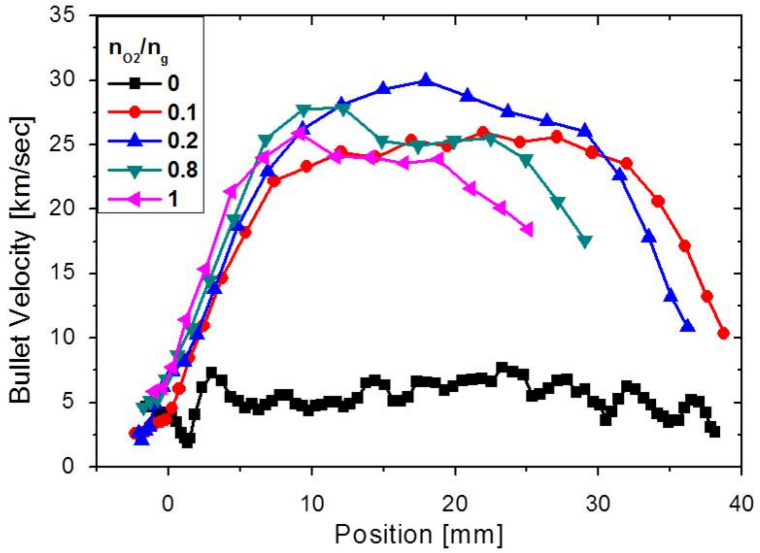


Figure 3.2 Bullet velocity in ambient $N_2/O_2$ mixture condition

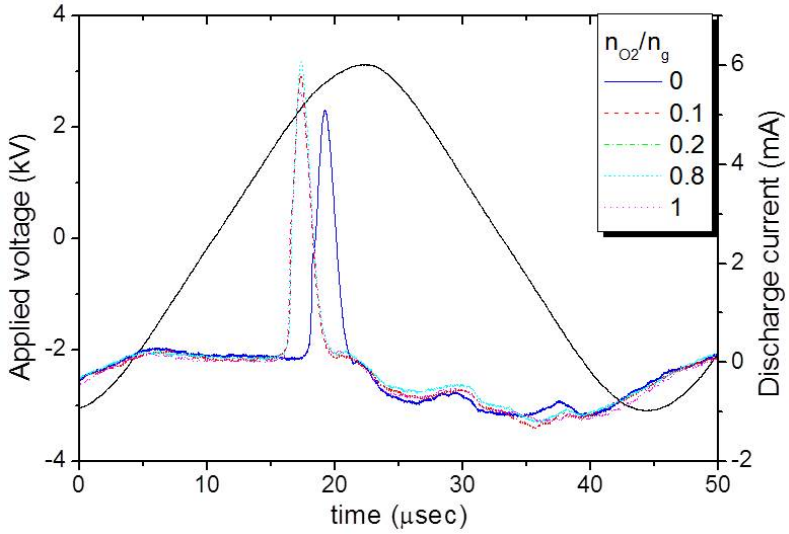


Figure 3.3 Applied voltage and discharge current in reactor

At the moment when the He gas breakdown occurs between the reactor electrodes, bullet speed is suddenly reduced and maintained constant during the reactor discharge.

According to this result, it can be inferred that the bullet propagation speed depends on the discharge in reactor. The time or amplitude of reactor discharge can be controlled by varying the distance of electrodes because the electric field between electrodes is determined by the distance between them. The shorter distance of reactor electrodes are, the faster source discharge occurs and then the more extreme change of bullet velocity is caused. In Figure 3.4, the distance is 15 mm and in Figure 3.5 is 5 mm which is much shorter three times. Distribution of bullet velocity can be varied according to the reactor geometry. In spite of the different condition of applied voltage and frequency so the quite large difference of bullet velocity, note that the effect of reactor discharge on velocity distribution and phases are important. When the gap distance is 15mm, the discharge at the edge of power electrode begins earlier than between the power and ground electrodes. In other words, there is a time lag between bullet discharge and reactor discharge as shown in Figure 3.4. In contrast, when the electrode distance is 5mm, reactor discharge and bullet propagation are coincided but the currents are opposite. As in Figure 3.5, the time of bullet generation and reactor discharge is similar. When the Reactor discharge is on, bullet is located at 2 mm from the tube exit where it is very close to the reactor,

so the velocity dramatically decreases due to opposite electric force of reactor discharge. During the reactor discharge, bullet velocity is constant and recovered to the initial value after the reactor discharge starts to decrease. The decreasing and increasing rates of bullet velocity are approximately same, $2.5\times10^{9}\ m/s^{2}$. It implies that there is a force balance between bullet electric field at head and induced electric field from charges of reactor discharge. That is, the time difference between bullet propagation and reactor discharge which can be controlled by electrode distance affects the bullet velocity distribution in space, the peak velocity and whole jet length. It is clear that reactor discharge makes opposite electric field that drags the bullet propagation from the discharge currents and bullet velocity distributions.

Figure 3.6 shows the relation between change of bullet propagation phase at B point and reactor discharge with various ambient mixture conditions. Except $n_{O2}/n_g$= 0 condition, the bullet velocities are decreased when discharge breaks down in reactor and bullets enter into the phase 2.

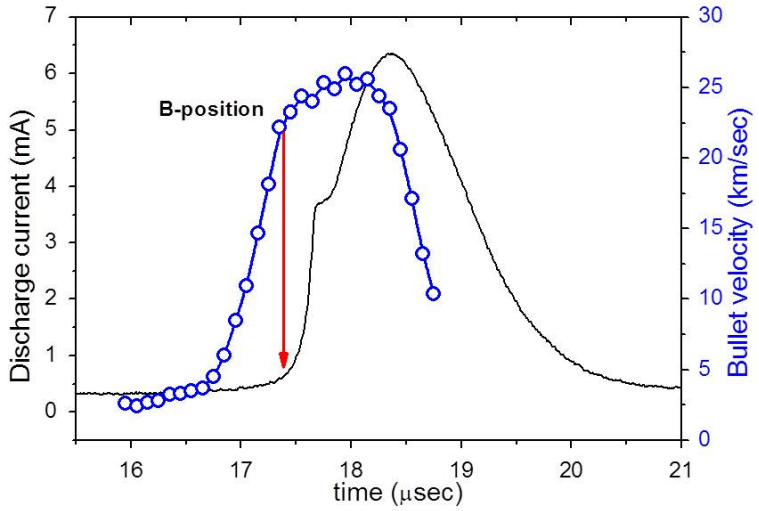


Figure 3.4 Discharge current and bullet velocity with $N_2$:$O_2$ = 4:1 condition ($n_{O2}/n_g$=0.2)

: Applied voltage and frequency are 6.3 kVpp and 22 kHz. He mass flow is 1 lpm

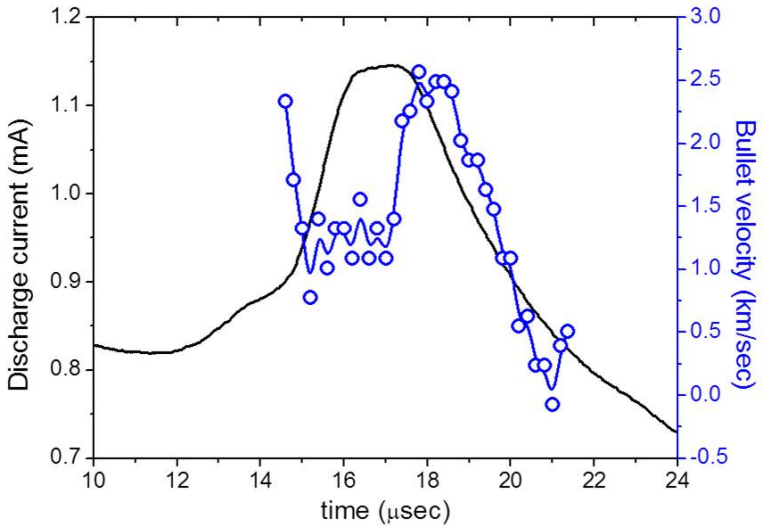


Figure 3.5 Discharge current and bullet velocity in ambient air

: Applied voltage and frequency are 8 kVpp and 10 kHz. He mass flow is 2 lpm.

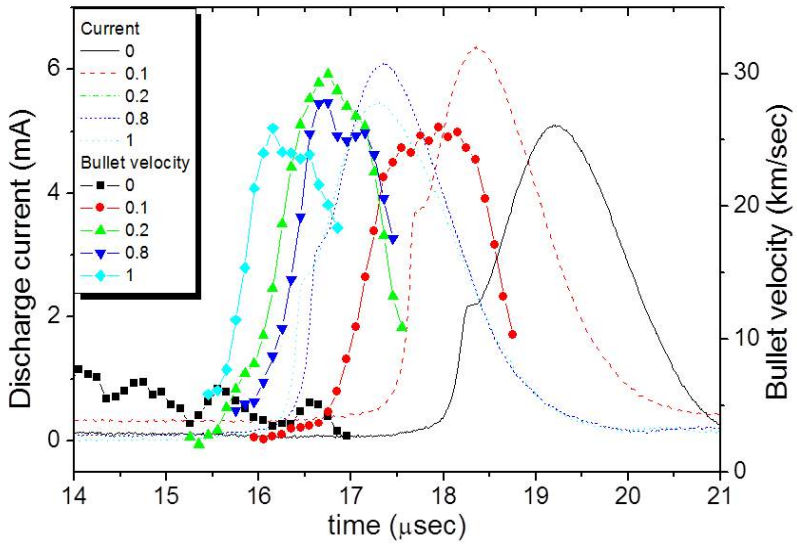


Figure 3.6 Reactor discharge and bullet velocity in various ambient mixtures

## 3.2 Optical Emissions from APPJ Plume

Optical emission spectrums along the position at 1, 3, 5, 7, 10, 15 and 20 mm from quartz exit are acquired for measuring the major excited and ionized species. The intensity should be corrected because there are dark signals and grating sensitivity. Dark signals are generated from other light sources like lamp tubes in laboratory and natural through windows. 1200 groove grating is used in this experiment and it has different sensitivities according to the wavelength. Therefore the correction factor should be calculated from the standard light source. The measured intensities were abstracted and multiplied by dark signal and correction factor. The corrected and normalized intensity is shown in Figure 3.7. The major emissions are from $N_2$ excited species. OH and H radicals from dissociated $H_2O$, $O^*$ radical from $O_2$ and $He^*$ are detectable.

In next chapter, the velocity model based on the bullet propagation mechanisms and experimental results will be presented. Three of bullet propagation phases will be analyzed with this model in following chapters.

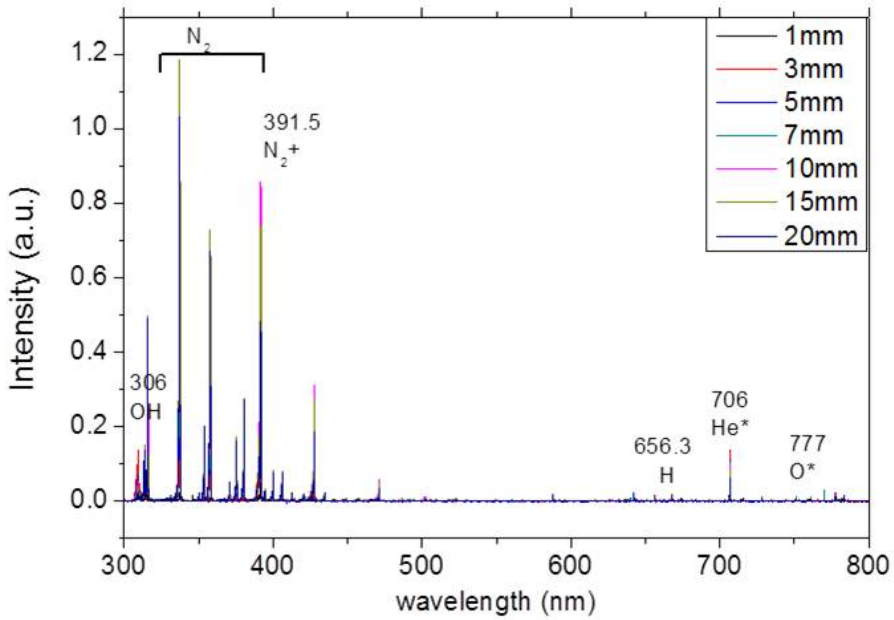


Figure 3.7 Full spectrum from 300 to 800 nm along the plasma plume in ambient air condition

# Chapter 4

# Discussion

## 4.1 The Bullet Velocity Model

Numerical modellings of bullet propagation in ambient air have been suggested by using plasma fluid dynamics in [9], [11] and [12]. These results are fitted well when the applied voltage is pulse shape with very short rise time (~20 nsec) and the amplitude is around 10 kV like in [13]. According to [13], the bullet velocity is about $5\times10^2$ km/sec. In case of sine wave and low voltage amplitude around 3~4 kV, the bullet velocities are around 10 km/sec which is lower 50 times than the former. Although bullet propagation velocities have three phases along the plasma plume in our experimental results and [6], the numerical simulation results cannot explain these phases and the velocity order of several km/sec.

To find out the effects of ambient gas condition and reactor

discharge on bullet propagation, simple analytic model can be suggested. Cathode-directed streamer propagation is maintained by avalanche of seed electrons in front of streamer and the streamer head is defined where avalanche-to-streamer transition occurs [14]. In bullet head, electron avalanche occurs due to the positively charged bullet head so it can be assumed that the bullet propagation is similar to the streamer. At streamer head, electron drift velocity by head electric field ($v_e = \mu_e E$) has relevance to its velocity. Streamer velocity depends on the external electric field and it can be faster or slower than electron drift velocity according to the external conditions. In low or no external electric field, electron drift velocity is an upper limit of streamer velocity [15]. For the bullet which propagates in free space with no biased or grounded substrates, the velocity cannot exceed the electron drift velocity at bullet head. So the estimation of bullet velocity from electron drift velocity may overestimate the experimental results. To improve the assumption that electron drift velocity indicates the bullet velocity, bulk structure of bullet head shown in Figure 4.1 and equation (4.1) propagating with velocity $v_b$ is assumed.

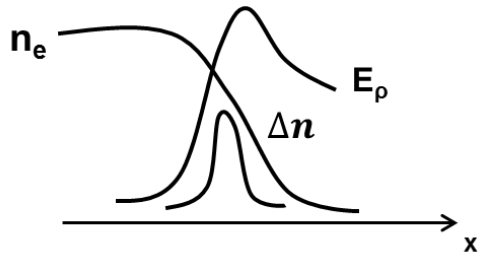


Figure 4.1 Structure of bullet head: Distribution of electron, space charge and its electric field

$$\begin{aligned} n_e &= n_e(x - v_b t) \\ \Delta n &= \Delta n(x - v_b t) \\ E_\rho &= E_\rho(x - v_b t) \end{aligned} \tag{4.1}$$

where $n_e$ , $\Delta n$ and $E_\rho$ are the electron, the space charge density and the electric field due to space charge respectively. In addition, penning, e−n collision ionization and electron attachment to $O_2$ are considered in particle balance of electrons, positive and negative ions to consider the electron generation and loss processes in equation (4.2).

$$\begin{aligned} \frac{\partial n_e}{\partial t} + \nabla \cdot \Gamma_e &= \upsilon_i n_e + \sum_j K_{pen,j} n_j n_{He^m} - \beta n_e n_+ - \eta n_{O_2} n_+ \\ \frac{\partial n_+}{\partial t} + \nabla \cdot \Gamma_+ &= \upsilon_i n_e + \sum_j K_{pen,j} n_j n_{He^m} - \beta n_e n_+ \\ \frac{\partial n_n}{\partial t} + \nabla \cdot \Gamma_n &= \eta n_{O_2} n_+ \end{aligned} \tag{4.2}$$

$\Gamma_l$, $\upsilon_l$, $K_{pen,j}$, $n_j$, $\beta$ and $\eta$ are fluxes of particle l, e−n collision ionization frequency, reaction rates of penning ionization of j molecule by $He^m$, recombination rate and attachment rates which include both attachment and dissociative attachment producing $O_2^-$ and $O^-$ respectively.

Because the diffusion coefficient and mobility of positive and negative ions are much smaller than electron [16] about 100 times, ion fluxes due to diffusion and drift can be ignored. It can be assumed that the ions are immobile to the bullet head and external electric field. Electron diffusion can be also ignored even though the electron density gradient is quite large due to the local high electric field.

Two kinds of electric fields that affect the electron motion can be considered in bullet propagation: First, space charge electric field ($E_\rho$) at bullet head and second, Laplacian field ($E_L$) due to applied voltage ($E_A$) and reactor discharge ($E_d$). Because $E_A$ is about 0.1 kV/cm far smaller than $E_\rho$ and $E_d$, field of applied voltage can be ignored. From the particle balance equation shown in equation (4.2) with electric field conditions, current continuity equation is derived as (4.3)

$$\frac{\partial}{\partial z}(ev_b\Delta n + ev_L n_e - en_e v_e) = 0 \qquad (4.3)$$

The first term $ev_b\Delta n$ means displacement current by moving space charge of bullet head. Second term $ev_L n_e$ is electron flow due to external electric field from reactor discharge. The last

term $en_e v_e$ is electron mobility flow due to bullet head electric field. The external and bullet head electric field is assumed as $\frac{Q_{in}}{4\pi\varepsilon_0 z_b^{\,2}}$ and $\frac{e\Delta nR}{3\varepsilon_0}$ where $Q_{in}$ [C], $z_b$ [m] and $R$ [m] is produced charges due to reactor discharge, distance from power electrode to bullet head and radius of spherical bullet respectively. Therefore the electron velocity, $v_L$ and $v_e$ can be obtained by multiplying electron mobility to electric field so $\mu_e \frac{Q_{in}}{4\pi\varepsilon_0 z_b^{\,2}}$ and $\mu_e \frac{e\Delta nR}{3\varepsilon_0}$ . From the equation (4.3), bullet velocity then,

$$\begin{aligned} v_b &= \frac{n_e}{\Delta n}(v_e - v_L) \\ &= \frac{e\mu_e R}{3\varepsilon_0} n_e - \frac{n_e}{\Delta n}\frac{\mu_e Q_{in}}{4\pi\varepsilon_0 z_b^{\,2}} \end{aligned} \tag{4.4}$$

The first term in RHS is related with electron drift velocity and proportional to electron density. Second term represents the effect of reactor discharge. To calculate the equation for estimating the bullet velocity, molar fraction of gas molecules along the plasma plume and plasma parameter such as electron mobility and collision reaction rates are essential. CFD-ACE+ which is the commercial code for computational fluid dynamics, provided by ESI group is used to compute the flow dynamics in plasma plume. Plasma parameters can be obtained by electron Boltzman equation solver, BOLSIG+.

When the ambient mixture ratio is changed, the molar fractions of each species along the bullet propagation are also

changed. To find out the quantitative relations between gases and propagation characteristics in three regions of bullet velocity, molar fractions of gases within the plume radius and length should be calculated. In Figure 4.2, conditions and geometry for simulation is shown. It is assumed that the system is cylindrically symmetric so the calculation region is limited by yellow box in Figure 4.2(a). The quartz radius and length are 1 mm and 35 mm and the left end of quartz tube is inlet boundary. Because all of experiments are conducted under with He 1lpm, the laminar flow, the boundary condition is set by normal inlet velocity, 8.5 m/sec and the turbulence mode was turned off. The radial size of ambient mixture region is 10 mm, enough for identifying the gas diffusions. The initial volume condition is 100% He inside the quartz tube and 100% $N_2/O_2$ gas mixture in ambient gas region.

The results of flow simulation are in Figure 4.3 and Figure 4.4. The maximum neutral flow velocity is about 9 m/sec at the very exit of quartz tube which is $10^3$ times slower than bullet propagation velocity. He, $N_2$ and $O_2$ molar fraction in $n_{O2}/n_g$=0.2 condition along the position at r=0.5 mm is in Figure 4.4(a). He diffuses out and $N_2$, $O_2$ entrains in with constant rates. According to the ambient $N_2$ and $O_2$ ratio, $O_2$ molar fraction is changed in same position as shown in Figure 4.4(b). When $O_2$ is 10% in ambient, $O_2$ molar fraction at r=0.5mm is only ~2%. However, when the ambient is filled with 100% $O_2$, its molar fraction at same position is over 20%.

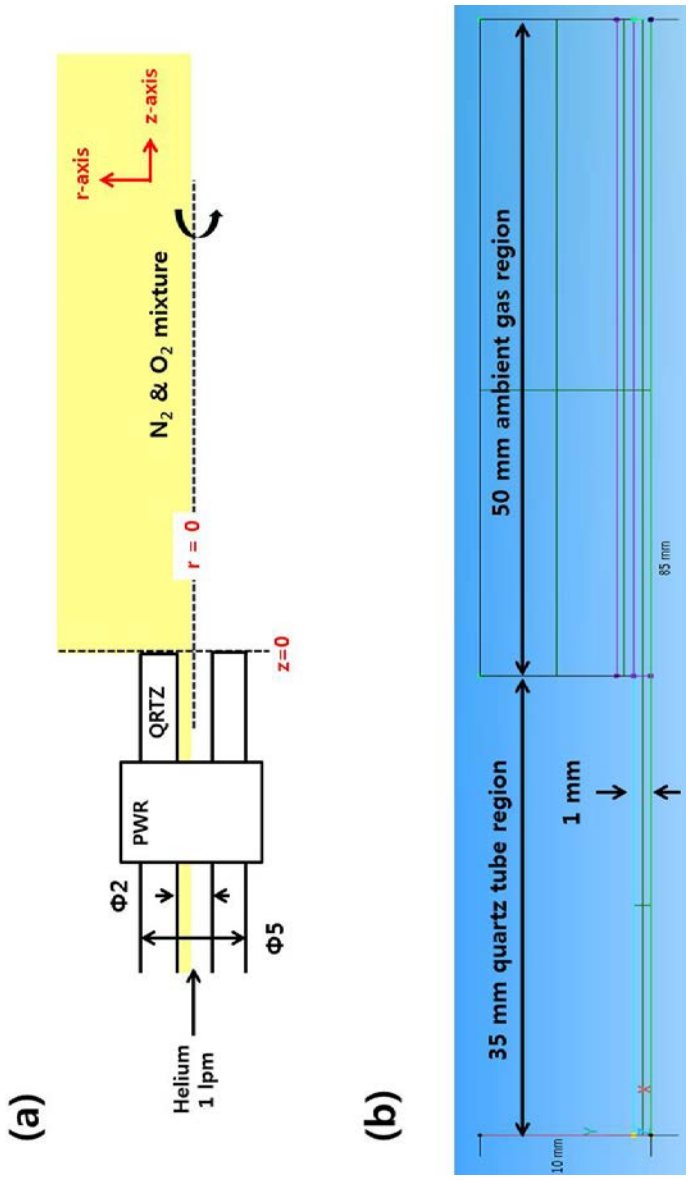


Figure 4.2 Schematic diagram for neutral gas flow simulation by using CFD-ACE+

(a) Experimental geometry of quartz tube and simulation region. Yellow box is calculated zone with axis symmetric. (b) Boundaries of calculation region in CFD-ACE+

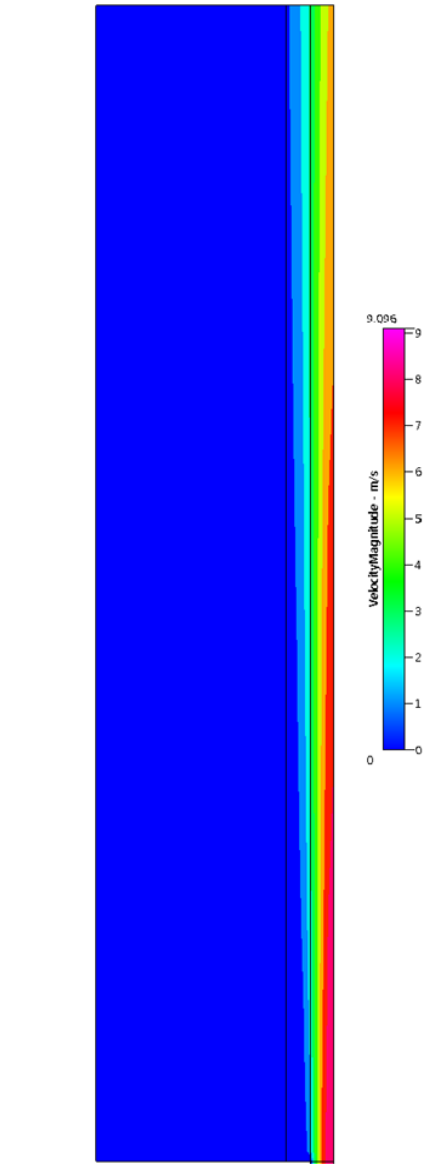


Figure 4.3 Neutral gas velocity along the plasma plum in dry air

: Inlet He flow rate is 1 lpm, and ambient N2/O2 mixture is 4:1

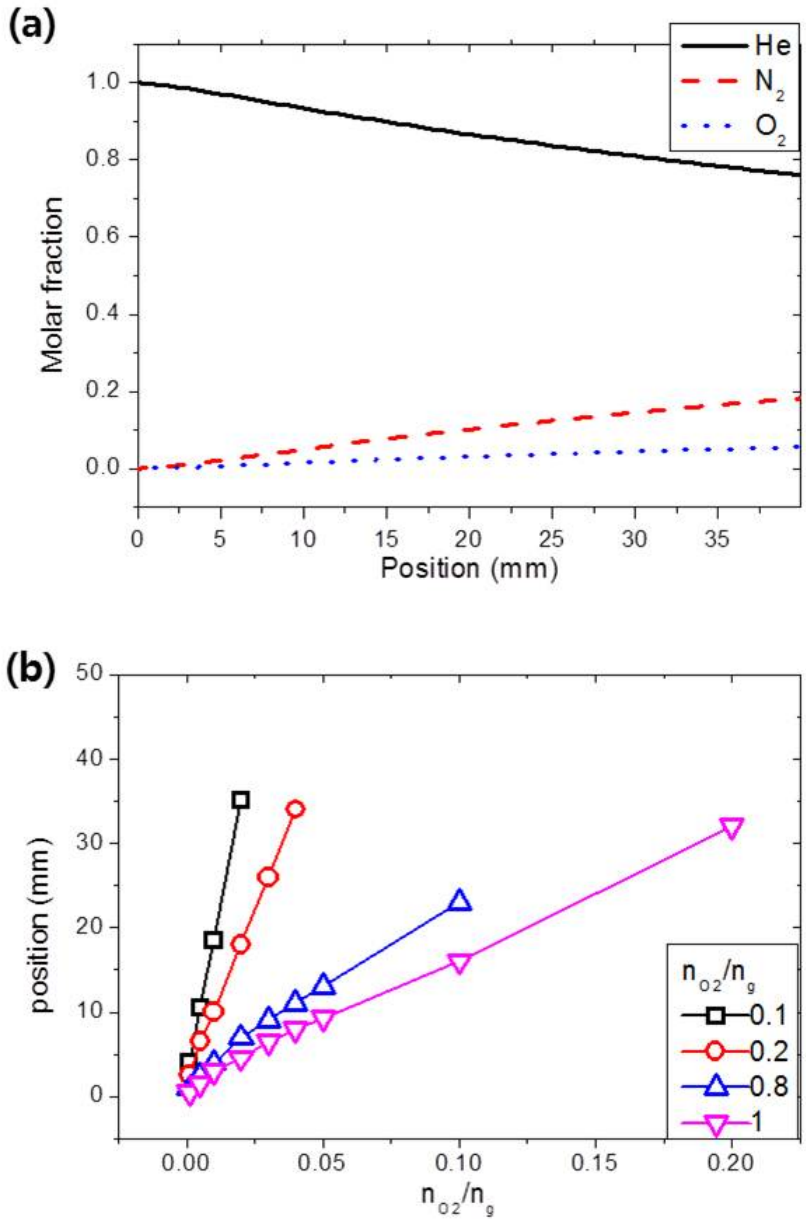


Figure 4.4 The results of gas flow simulation using CFD-ACE+

: (a) He, $N_2$, $O_2$ molar fraction in $n_{O2}/n_g$=0.2 condition at r=0.5 mm and (b) $O_2$ molar fraction at r=0.5mm position with various ambient mixture

For the plasma parameters such as e−n collision rates and electron mobility, BOLSIG+, open source cord in web, is used. Gas molar fraction and e−n collision reactions are required to calculate the Boltzman equation. The results of CFD−ACE+ and reactions provided by BOLSIG+ are used as the input parameters in BOLSIG+.

## 4.2 Bullet Velocity in Phase 1 : Acceleration Region

Helium excitation states and $N_2^+$ species emit 706 nm and 391.5 nm as in Figure 4.5. Because $N_2^+$ is produced by Penning ionization, higher 391.5 nm intensity represents more Penning reactions occurred in that position. In contrast, $He^*$ density would be decreased as penning becomes faster. So the line ratio of 391.5 nm and 760 nm qualitatively represents the degree of penning ionization. This line ratio and bullet velocity along the position are shown in Figure 4.6, as in phase 1 where the bullet is accelerated, the line ratio increases and saturated in phase 2 and 3. It can be deduced that the Penning ionization of $N_2$ by $He^m$ is the dominant effect on bullet acceleration.

Figure 4.7 shows the normalized intensities from each excitation species of He, O and $N_2$. The region is classified with numbering 1, 2 and 3 according to the characteristics of intensities trend, and bullet phases which corresponds to the numbering are presented at the top of the Figure 4.7. In region 1, where the vicinity of tube exit so $O_2$ molar fraction is too small, excited $N_2^+$ as well as He increases. In region 2, excited $N_2^+$ and O increase rapidly in contrast $He^*$ decreases. In region 3, all the intensity of excited species decrease with a similar rate. From these experimental results, excited species of ambient gases are governed by $He^m$ and the Penning reactions

between $He^m$ and ambient gases are dominant in Phase 1.

Since e−n collision also results in ionization of $N_2$ and $O_2$, comparison between penning and e−n collision ionization is required for identifying what the main mechanism of bullet propagation in phase 1 is. Because the $He^m$ has enough energy to ionize the $N_2$ and $O_2$, the major products from Penning are $N_2^+$ and $O_2^+$. Note that these ionized species also can be produced from e−n collisions. Because the dissociative recombination of $O_2^+$ and electron is very fast reaction [17] so the $O^*$, the product of this process, can be considered as the results of Penning and e−n collision ionization. In spite $N_2^+$ and $O^*$ can be generated through both penning and e−n collisions, $N_2^*$ and $O_2$* species are only from the e−n collisions. These relations are arranged in the Table 2.

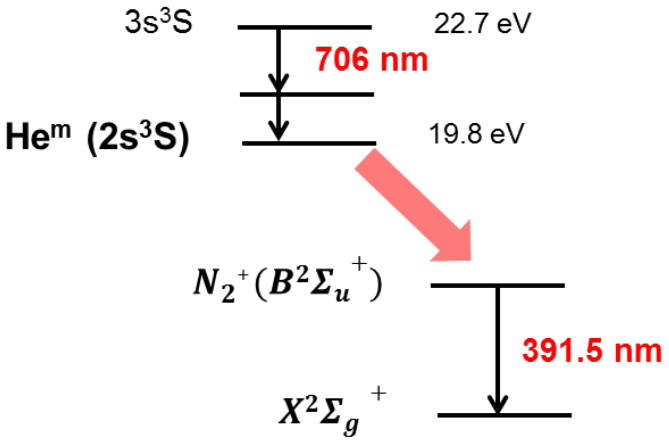


Figure 4.5 Emission lines from excitation state of He and $N_2^+$

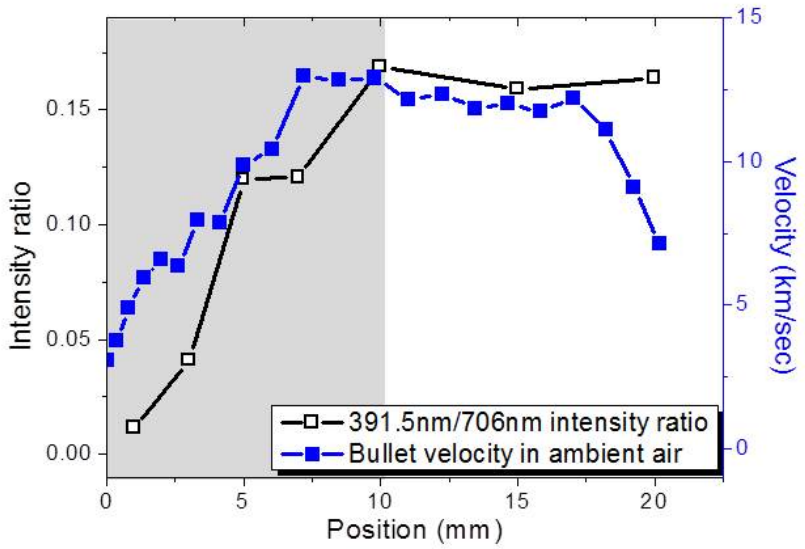


Figure 4.6 706nm 391.5 nm from He and $N_2^+$ emission line ratio and bullet velocity

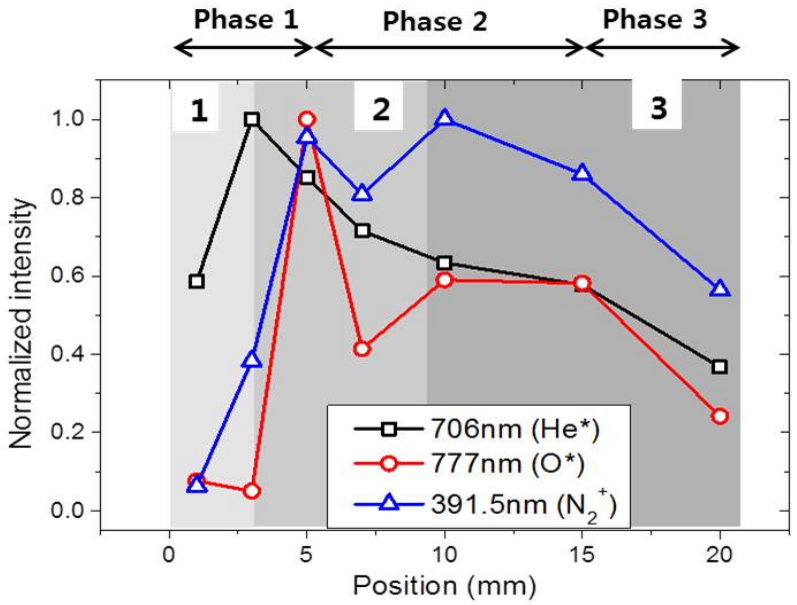


Figure 4.7 Normalized intensity distribution of He, O and $N_2$ excited states along the position

Table 2 Wavelength of each species and the production process of $N_2$, $O_2$ excited and ionized species

| | $N_2^+$ | $N_2^*$ | $O_2^*$ | $O^*$ |
|---|---|---|---|---|
| λ (nm) | 391.5 | 316/ 380.5 | 760 | 777 |
| Penning | ○ | X | X | ○ |
| e−n coll. | ○ | ○ | ○ | ○ |

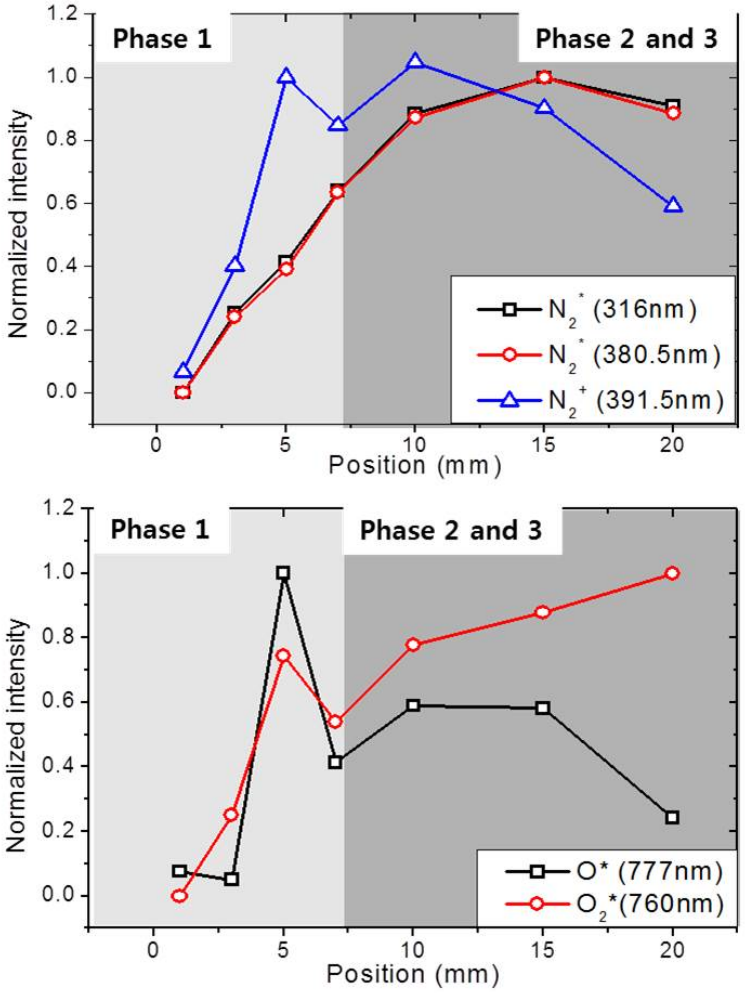


Figure 4.8 Normalized intensity distributions of (a) $N_2$ species and (b) $O_2$ and O

In Figure 4.8, normalized intensities from $N_2$, $N_2^+$, $O_2$ and O excited species are compared. In phase 1 where the bullet velocity increases, intensities of all of species are increased. However, in phase 2 and 3, intensities have different trends: products from the Penning reactions are weakly decreased as shown in He 706 nm dose. The products from the e−n collision excitations are slightly increase or maintain the maximum value. These results confirm that $N_2^+$ and $O^*$ are produced from Penning and they are relevant to the result of He 706 nm shown in Figure 4.7. Therefore it can be inferred that the Penning ionization is more dominant process in phase 1 and e−n collisions are concern in whole phases. To compare the degree of reactions in phase 1, reaction frequencies that the number of reaction in unit time can be used and obtained from $\upsilon = K_j n_j$ where $K$ is reaction rate.

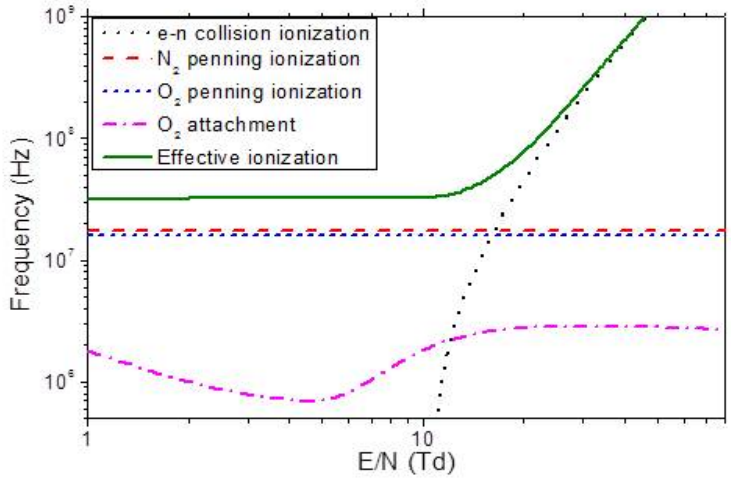


Figure 4.9 e−n collision, penning ionization, attachment and effective ionization frequency

The results are shown in Figure 4.9 at the middle of phase 1 in $n_{O2}/n_g$=0.2 ambient mixture condition. The densities of $He^m$ and electron, which have the energy for the reactions are assumed to be a similar value as $n_{He^m}/n_e \sim 1$. Due to the e−n collision reaction rates are function of E/N, the electric field at the position is needed.

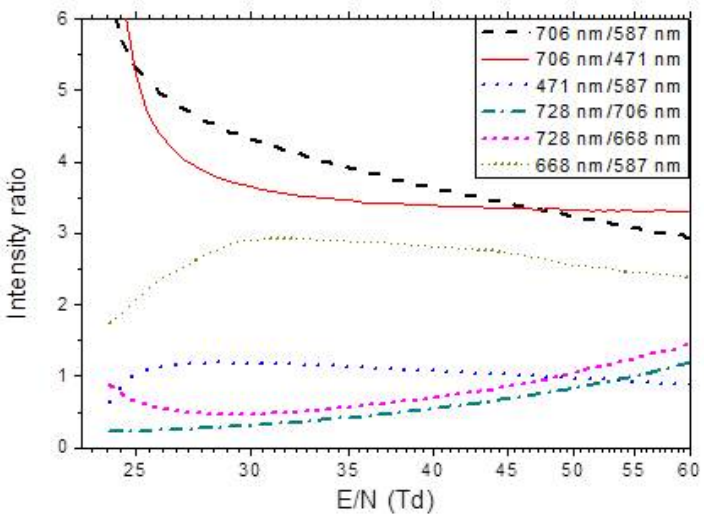


Figure 4.10 Intensity ratio of excited He from equation (4.5)

To estimate bullet electric field, optical emission line ratio from excited He is used. The uncertainties of equipment and experiments are offset each other so the line sensitivities according to the wavelength have only to be considered. $N_2$ and $O_2$ are excited by $He^*$ species as well as electrons, they are not proper to estimate the electric field. It is assumed that radiative loss is dominant and the plasma is optically thin because the radial size of the plume is ~1 mm in which the possibility of re−

absorption of radiations is low. The intensity ratio between p and k state of He is,

$$\frac{I_p}{I_k} = \frac{\int f_p(E) < \sigma v >_p dE}{\int f_k(E) < \sigma v >_k dE} \tag{4.5}$$

where $f(E)$ is electron energy distribution function. Because the collision frequency is really high in atmospheric pressure, electron energy is determined by reduced electric field so the equation (4.5) becomes the reaction rates corresponding to each energy level state. From the emission spectrum, 471 nm, 587 nm, 668 nm, 706 nm and 728 nm from $He^*$ can be detectable. Intensity ratios calculated by using BOLSIG+ and estimated electric field of bullet is shown in Figure 4.10. This method is not sensitive to measure the precise electric field because the ratios are diverge or cannot be calculated below 25 Td, but the range of the average electric field of plume along position can be assumed. The estimated electric field from selected line ratio, 668 nm/587 nm and 706 nm/471 nm, is shown in Figure 4.11 and it is found that the reduced field is in the rage of 23~25 Td (5~6 kV/cm). In this electric field regime, the effects of penning and e-n collision ionization are comparable and the attachment loss can be ignored. If the mixture composition condition is changed as the bullet position is located further, the reaction frequencies and relative degree of them will be changed. The details of phase 2 and 3 will be discussed in next chapter.

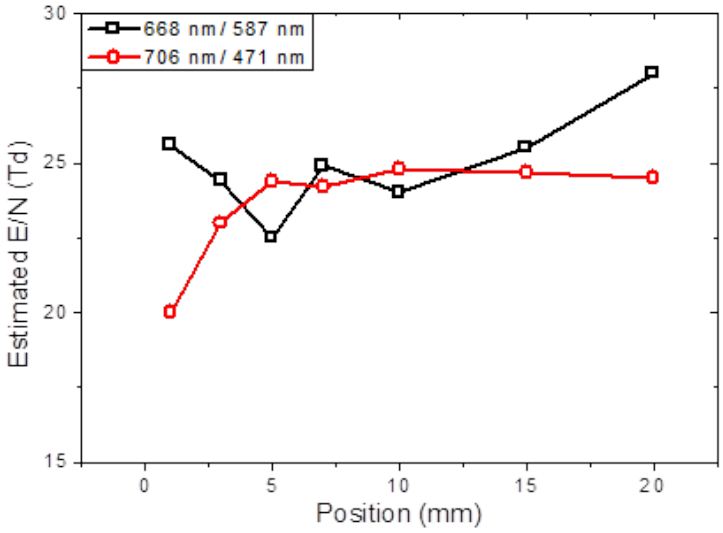


Figure 4.11 Estimated electric field of bullet by using intensity ratio of He excited states

As a result of reactions presented in Figure 4.10, the electron density is determined. According to the bullet propagation equation (4.4), the velocity is proportional to electron density when there is no reactor discharge, that is $Q_{in}$=0. Electrons are generated through e−n collision and penning ionization process and loose by $O_2$ attachment. If the time scale is 10 ~ 50 nsec, which is enough to collision reactions and satisfies to regard bullet as in steady position, time variation of electron density can be presented as below.

$$\frac{\partial n_e}{\partial t} = \overline{\upsilon_i} n_e + \sum_j K_{pen,j} n_{He^m} n_j - K_{att} n_{O_2} n_e \qquad (4.6)$$

$$n_e = n_{e0} e^{(\overline{\upsilon_i} + \frac{n_{He^m}}{n_e}\sum_j K_{pen,j} n_j - K_{att} n_{O_2})t}$$

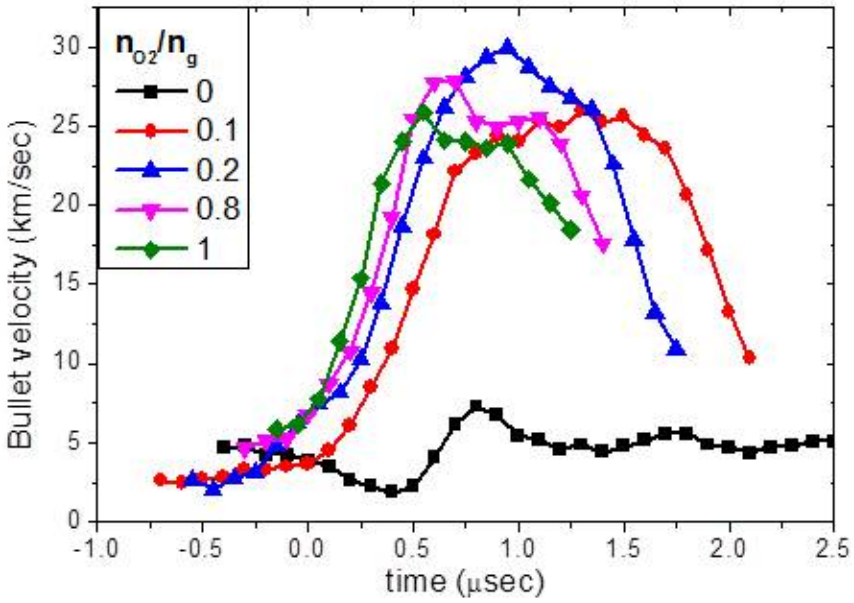


Figure 4.12 Bullet propagation velocity with time scale

Collision frequencies in equation (4.5), which is the exponential factor, are calculated as in Figure 4.9 with proper gas mixture conditions, with a function of reduced electric field. Electron density grows exponentially in time scale then the bullet velocity is

$$v_b = \frac{e\mu_e R}{3\varepsilon_0} n_{e0} e^{(\bar{\upsilon}_i + \frac{n_{He^m}}{n_e}\sum_j K_{pen,j} n_j - K_{att} n_{O_2})t)} \tag{4.7}$$

Phase 1 is defined where the bullet velocity increases linearly according to the position in chapter (3.1) and as shown in Figure 4.12. Relation between velocity-position can be transformed to velocity-time then the time variation of bullet velocity is

$$\frac{\partial v_b}{\partial z} = \frac{1}{v_b}\frac{\partial v_b}{\partial t} = C \tag{4.8}$$

where C is velocity slope of phase 1 in position scale. It can be found from equation (4.7) that bullet velocity also exponentially increases in experiment,

$$v_b = v_{b0} e^{t/\tau} \tag{4.9}$$

where $\tau$, a reciprocal of C, is characteristic time of velocity increase. Initial bullet velocity $v_{b0}$ is determined by electron mobility and initial electron density because $v_{b0} = \frac{e\mu_e R}{3\varepsilon_0} n_{e0}$ from equation (4.6). $v_{b0}$ can be assumed as a function of $n_{e0}$ because $\mu_e$ and R would be independent on ambient mixture ratio and the molar fraction of $N_2$ and $O_2$ is negligible as less than $10^{-5}$ at vicinity of tube exit. The ratio of $O_2$ and $N_2$ changes the local photoionization rate with linear proportionality. The electron sources by photoionization are proposed by H.-E. Wagner et. al. as following,( [18])

$$S_{ph}(\vec{r}) = \frac{\xi A(p)}{4\pi} \int \frac{h(p|\vec{r} - \vec{r}'|) S_i(\vec{r}') d^3(p\vec{r})}{\left| p\vec{r} - p\vec{r}' \right|^2} \tag{4.10}$$

$$h(p_{O_2} r) = \frac{e^{(-\kappa_{\min} P_{O_2} r)} - e^{(-\kappa_{\max} P_{O_2} r)}}{r \log(-\kappa_{\max} / \kappa_{\min})} \tag{4.11}$$

with $A_p = p_q / (p + p_q)$. $p_q$ is quenching pressure by collisions

with neutrals, $h(p_{O_2}r)$ is absorption function of photo-ionizing radiation and $\xi S_i$ is local impact ionization rate. $h(p_{O_2}r)$ increases as oxygen pressure so the initial electrons would be increased due to the photoionization of $O_2$. When $\mu_e$~0.085 and R=1 mm is assumed, the initial electron density and $h(p_{O_2}r)$ factor can be estimated as in Figure 4.13. The initial electron densities are increased rapidly when $n_{O2}/n_g > 0.2$. Even though $h(p_{O_2}r)$ factor cannot explain the sudden increase of electron density at $n_{O2}/n_g=0.2$ condition, photoionization can be a candidate of increment of initial electron density as higher $O_2$ fraction in ambient gas. However the initial bullet velocity is closely related to the surface discharge, mostly at the edge of tube, so it is required further studies to elucidate the details.

Returning to subject, exponential growth of bullet velocity is expected from both the model and experimental results. The characteristic time scale of growth can be obtained by exponential fitting from experimental results. If bullet electric field is assumed to 25 Td, normalized effective ionization frequency and C, which is the exponent part of the model and measured bullet velocity respectively, is compared in Figure 4.14. The model expects the experimental results well. In phase 1, acceleration rates of bullet propagation increase as ambient $O_2$ molar fraction since electron loss rate due to attachment is far less than the production rates and penning, e-n collision ionization increases as $n_{O2}/n_g$.

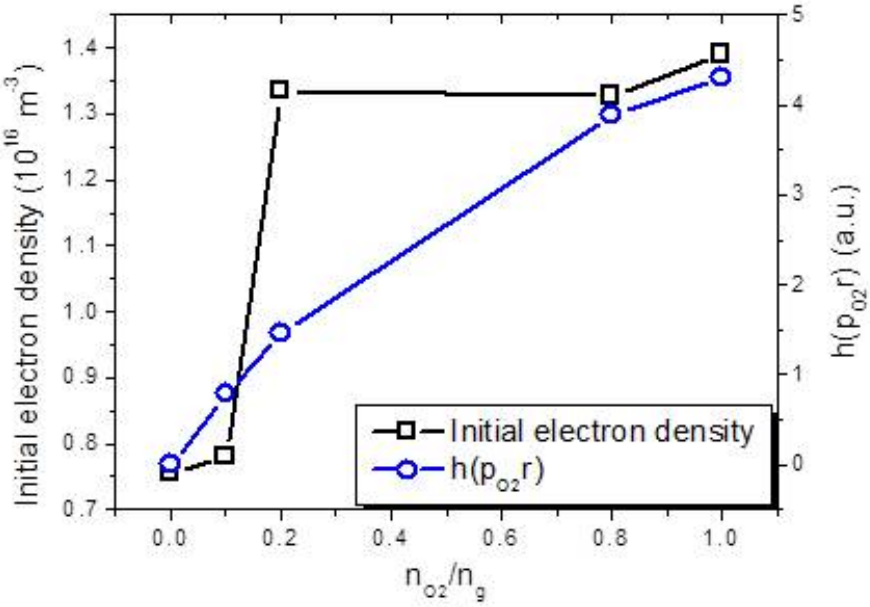


Figure 4.13 Initial electron density and h($p_{O2}$r)

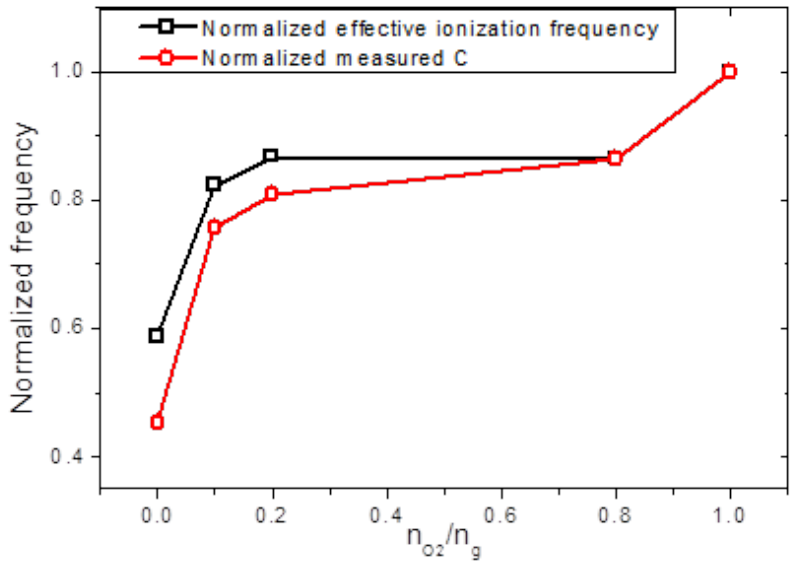


Figure 4.14 Comparison between normalized effective ionization frequency (E/N=25 Td) and C from measured bullet velocity

## 4.3 Bullet Velocity in Phase 2 : Constant Velocity Region

Phase of bullet propagation velocity is suddenly changed at B position. It is not common because variation of gas flow and molar fractions, main causes of bullet velocity, are continuous along the position. In section 3.1, it is suggested that this sudden change is due to the accumulated charge inside the quartz tube after the reactor discharge and the bullet velocity model reflects this relation through the external electric field. Unlike in phase 1, $Q_{in} \neq 0$ and the bullet velocity when $n_e / \Delta n \sim 1$,

$$v_e = \mu(E) \cdot \left(\frac{Q_{in}}{4\pi\varepsilon_0 z_b^{\,2}} + E_{bullet}\right) \qquad (4.12)$$

where $E_{bullet}$ is charge electric field at bullet head. $Q_{in}$ can be measured, $Q_{in} = C_{dum} \times V_{dum}$ where $C_{dum}$ and $V_{dum}$ are capacitance and voltage of dummy capacitor. Electron mobility can be calculated from BOLSIG+ and the results are shown in Figure 4.15 and Figure 4.16. At low E-field below 20 Td, the bullet velocity variation according to the ambient $O_2$ fraction is drastic. However as bullet electric field increases, the difference decreases. The bullet head electric field can be estimated to about 30 Td from Figure 4.16, similar but a little higher than one from OES shown in Figure 4.11, with 20% discrepancy. This discrepancy may be caused from the time averaged data of

OES. For the more accurate electric field, optical emission should be acquired during the triggered time with bullet generation.

Unless the electric force due to reactor discharge is considered, the estimated bullet velocities become identical to the electron drift velocity and three times faster than measured one. In contrast, with considering reactor discharge, bullet velocities cut down by 20 km/sec, about 30% of electron drift velocity (Figure 4.17).

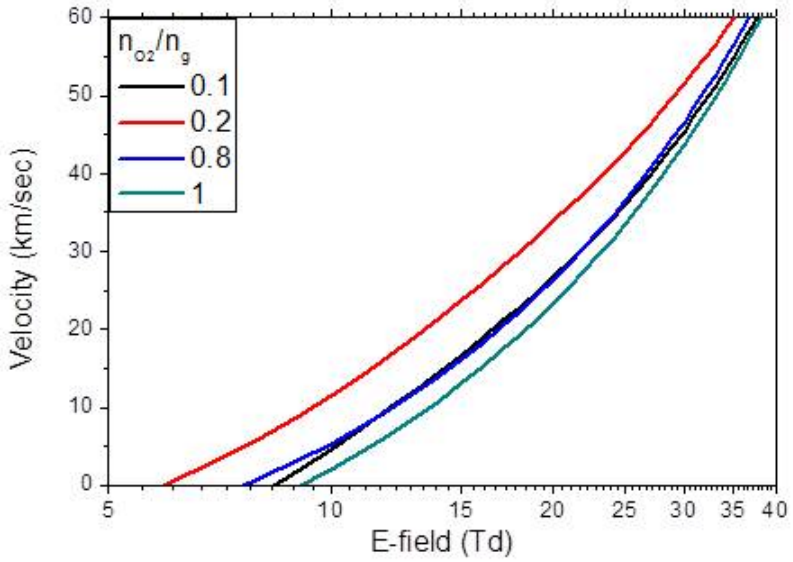


Figure 4.15 Estimated bullet velocity using equation (4.12) in phase 2

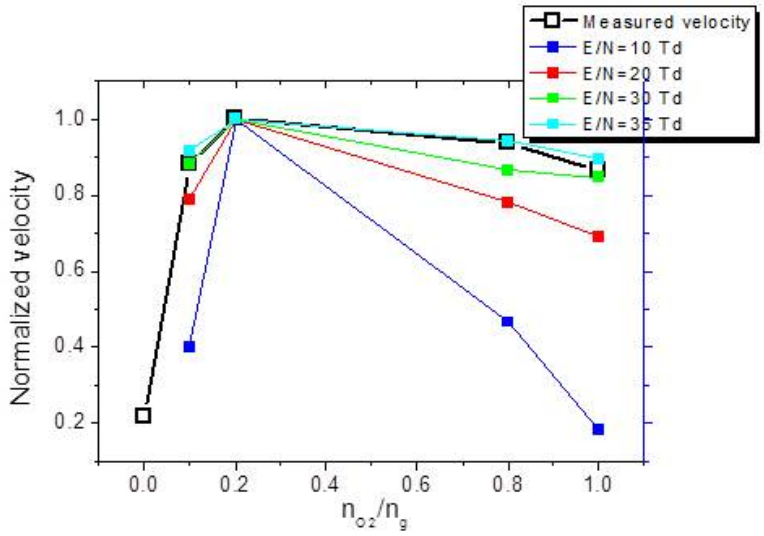


Figure 4.16 Comparison between measured bullet velocity and estimated one with various bullet E−field and ambient $O_2$ fraction

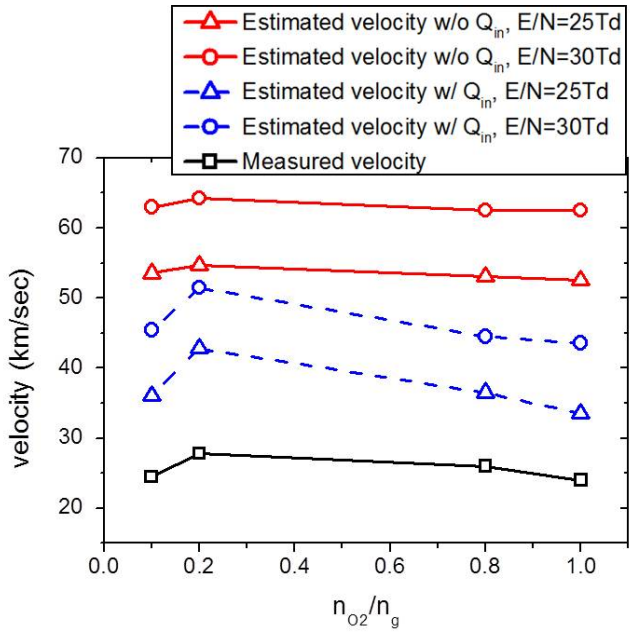


Figure 4.17 Estimated bullet velocity with and without considering accumulated charge due to reactor discharge

## 4.4 Bullet Velocity in Phase 3 : Deceleration Region

The more ambient $O_2$ is added, the shorter the length of phase 2 is. In other words, C position where the phase 3 starts approaches to B position and the variation of it is shown in Figure 4.18. Because the B position relatively constant regardless of $n_{O2}/n_g$, the length of phase 2 is linearly decreased. However, the He molar fractions at C have two groups, $n_{O2}/n_g \leq 0.2$, low $O_2$ and $n_{O2}/n_g \geq 0.8$, high $O_2$ regime at r=0 where the center of plasma plume and almost constant values in each group. $O_2$ gas in ambient air has two roles in bullet propagation, the one is penning ionization and the other is electron attachment. When the small amount of entrainment from ambient to plasma plume enhances the penning ionization rate because He metastable density still accounts lots of portion in that position. However, if the $O_2$ fraction becomes higher than critical value, electron loss by attachment is over than the generation by penning and e-n collisions. Figure 4.19 is reaction frequencies at C position when the ambient condition is $n_{O2}/n_g=0.2$, similar to dry air. From the estimated electric field from OES, it can be assumed that E/N is about 25 Td. In that field amplitude, electron number density may be constant because loss and generation is roughly similar. As bullet propagates father, electron loss increases due to increase of $O_2$ fraction and at the same time, generation decreases as a results

of decreased bullet electric field. In view of bullet velocity model, the time derivative of equation (4.4) is

$$\frac{dv_b}{dt} = \frac{e\mu_e R}{3\varepsilon_0}\upsilon_i n_{e0} e^{\upsilon_i t} \qquad (4.13)$$

Because $\upsilon_i$ is effective ionization frequency its value becomes negative mathematically when the loss is greater than the generation. Since $\frac{dv_b}{dt} \sim \upsilon_i$, bullet velocity varies linearly in phase 3 in contrast to the phase 1 where the velocity increase exponentially by the penning ionization.

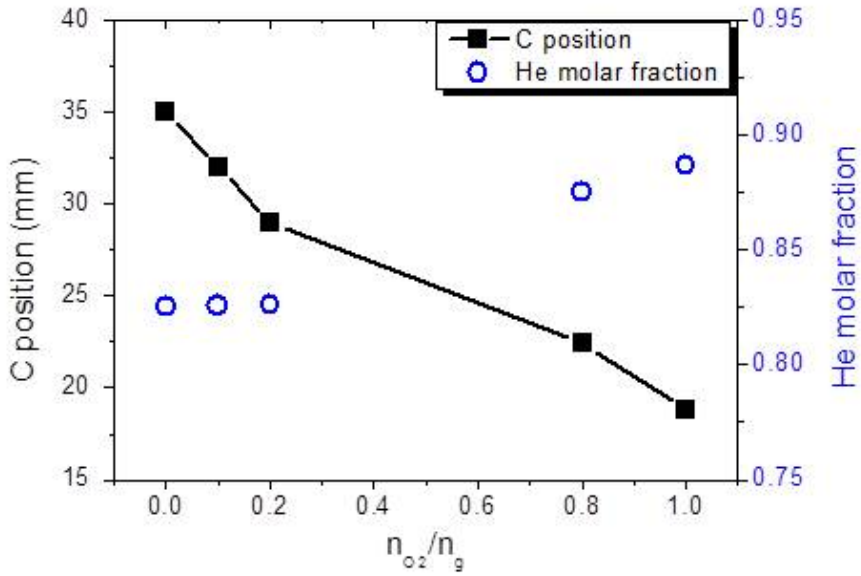


Figure 4.18 Limitation of He molar fraction at C position

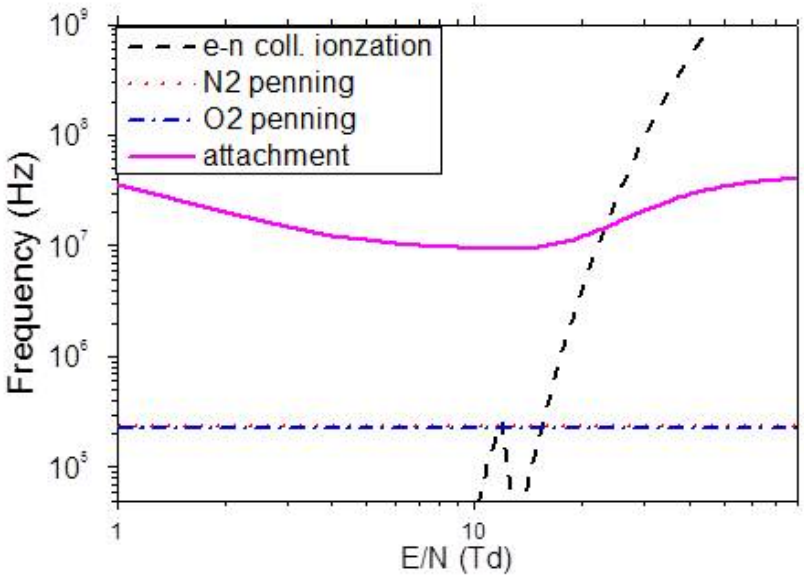


Figure 4.19 The e−n collision ionization, penning ionization and attachment reaction frequencies at C position ($n_{O2}/n_g$= 0.2)

The grounded metal substrate is located under the plasma plume for the simulation of the substrate treatment and the results are shown in the Figure 4.20. The applied voltage and frequency conditions are slightly changed for the stability of bullet when the substrate is under the plume. The distance from quartz tube exit to subtrate is 20 mm which is farther than jet length so the jet cannot contact with the substrate. In Figure 4.20 (a), the bullet propagations were not affected by discharges in reactor so the bullet velocity distributions have phase 1 and 3. When there is a grounded substrate under the plume, the image charges of bullet head on substrate make a

additional external electric field that enhances the bullet velocity. The maximum bullet velocity with substrate is greater than the bullet without substrate about two times as shown in Figure 4.20 (b). These results explain that the external electric field due to the substrate affect the bullet velocity. Most of the substrates for bio-medical applications may be the dielectrics so the position and dielectric constant of the substrate determine the amount of accumulated charges on it. The spacial distribution of bullet velocity can be changed according to the dielectric substrate position and the charge and radical fluxes are also changed because the induced electric field due to accumulated charge inhances the bullet velocity. In further studies, the dielectric substrate effects on the bullet velocity distribution to analyze the biological process results which are subject to the charge and radical fluxes.

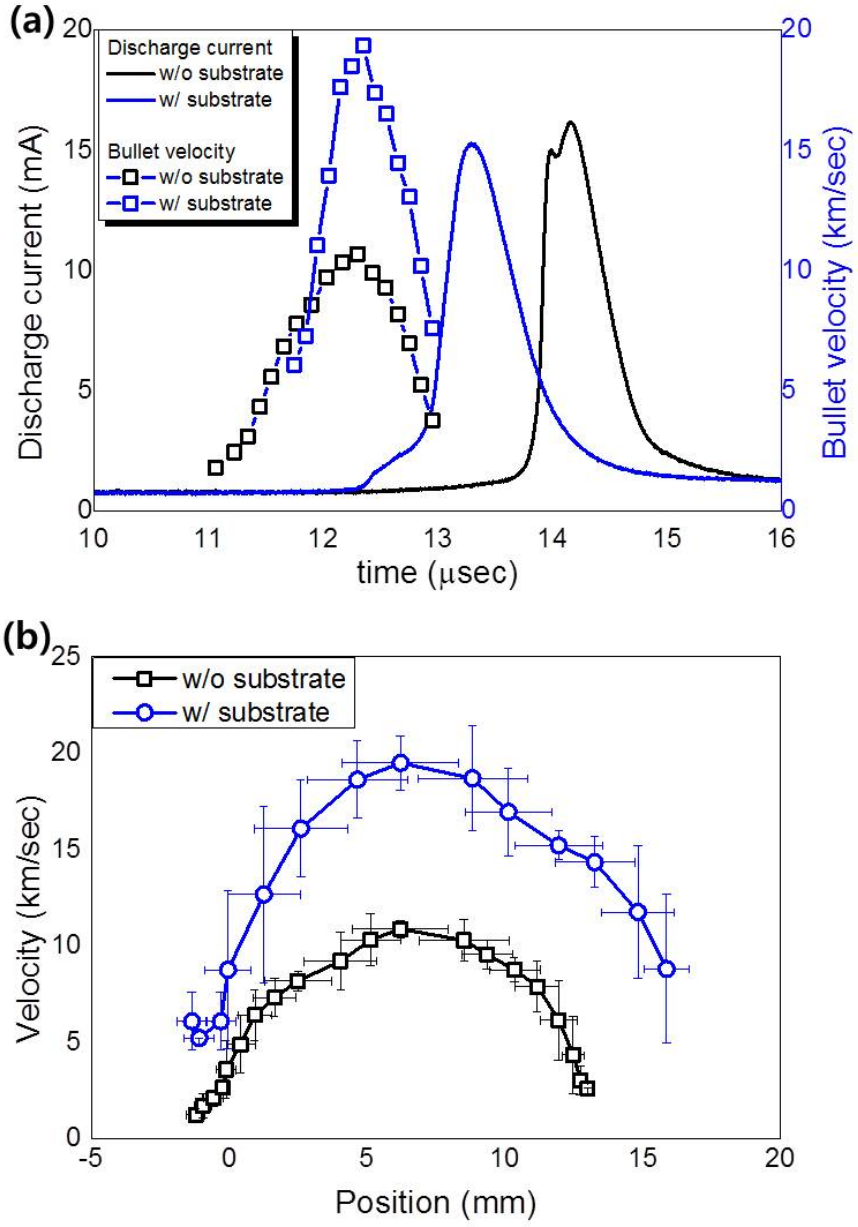


Figure 4.20 Bullet velocity with and without metal grounded substrate under the plasma plume

: Applied voltage and frequency is 7.3 kVpp and 18 kHz. (a) is bullet velocity and discharge current in time scale and (b)is bullet velocity in position scale.

# Chapter 5

# Conclusion

In spite of the factor that the bullet velocity has spatial distribution, it has not been concerned in APPJ applications. In this experiment, He-APPJ in controlled ambient condition is used to measure the distribution of bullet velocity by using ICCD images. Through the bullet velocity model as well as the results of electrical and optical measurement, the propagation mechanisms are explained along the position.

According to the bullet velocity measurement, it has three phases, which consist of acceleration (phase 1), constant velocity (phase 2) and deceleration phase (phase 3), regardless of ambient $O_2$ fraction. In phase 1, bullet velocity increases linearly with position and exponentially with time due to the increment of penning ionization and the negligible loss by electron attachment. It can be reconfirmed from OES data, the intensity ratio of 391.5 nm and 706 nm which is the emission

line of $N_2^+$ and $He^*$ respectively. In the region of phase 1, the intensity ratio of 391.5nm/706nm increases as bullet velocity does and it means the penning ionization rates increases in this region. From the bullet velocity model, the exponential growth of velocity with time is expected and the characteristic time scale for the growth is suggested as effective ionization frequency. The normalized effective ionization frequencies from the model with the various ambient $O_2$ fractions are well matched with the experimental results. In phase 2, the acceleration is suddenly decreased and becomes almost 0; constant velocity. The accumulated charges on quartz tube due to reactor discharge makes opposite electric field to the one of bullet head so the force balance between them results in the constant bullet velocity. In phase 3, bullet velocity starts to decrease linearly at certain position where the $O_2$/He molar fraction satisfies the condition that the electron loss rate by attachment surpasses the electron production rates from e−n collision and penning ionization. The C position where the phase 3 starts is brought forward as ambient $O_2$ fraction increases then the length of phase 2 is decreased. When the grounded metal substrate is located under the plume, the bullet velocity increases because the induced electric field by the image charges on substrate enhances the bullet propagation. Thus the dielectric substrate can affect the bullet velocity and the charge flux due to the accumulated charges on the dielectric and its induced electric field.

Spatial distribution of bullet velocity is subject to the ambient gas molar fraction and external electric field from reactor discharge, image charges on grounded substrate as well as electron density of bullet head. The effects of ambient gases and electric field have been qualitatively suggested before. Through the comparison between experiment results and bullet velocity model in each phase, quantitative analysis is conducted for the three phases along plasma plume. Charged particles and neutrals may have spatial distribution because of the particle densities are function of bullet electric field and velocity. To secure the reproducibility of experiments in applications using plasma products such as charged particles and neutral radicals from APPJ sources, controlled ambient conditions and proper treatment positions are required.

# References


[1] G. Y. Park, S. J. Park, M. Y. Choi, I. G. Koo, J. H. Byun, J. W. Hong, J. Y. Sim, G. J. Collins and J. K. Lee, "Atmospheric-pressure plasma sources for biomedical applications," *Plasma Sources Sci. Tech.,* vol. 21, p. 043001, 2012.

[2] M. Keidar, "Cold plasma selectivity and the possibility of a paradigm shift in cancer therapy," *British Jour. Cancer,* vol. 105, pp. 1295-1301, 2011.

[3] J. Schafer, R. Foest, A. Quade, A. Ohl and K.-D. Weltmann, "Local depoition of SiOx plasma polymer films by a miniaturized atmospheric pressure plasma jet(APPJ)," *J. Phys. D: Appl. Phys.,* vol. 41, p. 194010, 2008.

[4] X. Lu, M. Laroussi and V. Puech, "On atmospheric-pressure non-equilibrium plasma jets and plasma bullets," *Plasma Sources Sci. Tech.,* vol. 21, p. 034005, 2012.

[5] J. Shi and F. Z. J. Zhang, "A hypersonic plasma bullet train traveling in an atmospheric dielectric-barrer discharge jet," *Phys. Plasmas,* p. 013504, 2008.

[6] M. Laroussi, D. A. Mendis and M. Rosenberg, "Plasma interaction with microbes," *New J. Phys.,* vol. 5, pp. 41.1-41.10, 2003.

[7] E. Karakas, M. a. Akman and M. Laroussi, "Propagation phases of plasma bullets," *IEEE Trans. Plasma Sci.,* vol.

39, no. 11, 2011.

[8] E. Karakas and M. Laroussi, "Experimental studies on the plasma bullet propagation and its inhibition," *J. Appl. Phys.,* vol. 108, p. 063305, 2010.

[9] E. Karakas, M. A. Akman and M. Laroussi, "The evolution of atmospheric-pressure low-temperature plasma jets: jet current measurements," *Plasma Source Sci. Tech.,* vol. 21, p. 034016, 2012.

[10] G. Naidis, "Modelling of plasma bullet propagation along a helium jet in ambient air," *J. Phys. D: Appl. Phys.,* p. 215203, 2011.

[11] K. Urabe, T. Morita, K. Tachibana and B. N. Ganguly, "Investigation of discharge mechanisms in helium plasma jet at atmospheric pressure by laser spectroscopic measurements," *J. Phys. D: Appl. Phys.,* vol. 43, p. 095201, 2010.

[12] G. Naidis, "Simulation of streamers propagating along helium jets in ambient air: Polarity-induced effects," *Appl. Phys. Lett.,* vol. 98, p. 141501, 2011.

[13] A. Luque, V. Ratushnaya and U. Ebert, "Positive and negative streamers in ambient air: modelling evolution and velocities," *J. Phys. D: Appl. Phys.,* vol. 41, p. 234005, 2008.

[14] B. L. Sands, B. N. Ganguly and K. Tachibana, "A streamer-like atmospheric pressure plasma jet," *Appl. Phys. Lett.,* vol. 92, p. 151503, 2008.

[15] A. A. Kulikovsky, "Analytical model of positive streamer in weak field in air: Application to plama chemical

calculations," *IEEE Trans. Plasma Sci.,* vol. 26, no. 4, 1998.

[16] G. Dawson and W. Winn, "A model for streamer propagation," *Zeitschrift fur Physik,* vol. 183, pp. 159-171, 1965.

[17] X. Yuan and L. L. Raja, "Computational study of capacitively coupled high-pressure glow discharges in helium," *IEEE Trans. Plasma Sci.,* vol. 31, no. 4, 2003.

[18] Y. P. Raizer, Gas discharge physics, Springer, 1997.

[19] H.-E. Wagner, Y. V. Yurgelenas and R. Brandenburg, "The development of microdischarges of barrier discharges in N2/O2 mixtures- experimental investigation and modelling," *Plasma Phys. Control. Fusion,* vol. 47, pp. B641-B654, 2005.

[20] Y. Xian, X. Lu, Y. Cao, P. Yang, Q. Xiong, Z. Jiang and Y. Pan, "On plasma bullet behavior," *IEEE T. Plasma Sci.,* vol. 37, no. 10, 2009.

# 초 록

헬륨 상압 플라즈마 제트(He-APPJ)는 대기압의 조건에서 작동 가능하고 그 이용이 저압 플라즈마에 비해 간편하며 반응성이 큰 OH, $O_3$, NO와 같은 라디컬이 다량 생성된다는 장점을 가진다. 이로 인해 바이오, 의료 분야에서 살균, 암 치료, 미용 등의 목적으로 APPJ가 이용되고 있지만, 실험이나 치료 결과의 재현성이 떨어져 일정한 효과를 기대하기가 어렵고, 플라즈마와 처리 대상간의 상관관계를 도출하는 데 어려움이 있다. APPJ 소스는 주변 공기의 상태에 의해서 제트의 특성이 변할 수 있기 때문이며, 특별히 제트의 형상을 구성하는 불렛' 과 주변 공기와의 관계에 대한 이해가 선행되어야만 한다. 본 학위 논문에서는 주변 혼합 가스의 조건에 따라 변화하는 불렛 속도 및 불렛 진행 메커니즘에 대한 연구를 진행하였다.

헬륨 APPJ로부터 발생한 불렛은 주로 공기 중에서 진행하기 때문에 헬륨과 주변 질소, 산소와의 반응이 중요하다. 질소와 산소의 이온화 에너지는 헬륨 준안정준위 종의 에너지보다 낮아 페닝 이온화로 인하여 $N_2^+$, $O_2^+$ 등의 이온과 전자를 생성한다. 특히 산소는 페닝과 동시에 음이온을 생성하여 전자 밀도를 감소시키는 역할도 하기 때문에, 주변 가스 중 산소의 분율은 불렛의 전자 밀도 및 불렛 진행 속도에 영향을 준다. 본 실험에서는 외부 공기와 차단된 챔버 내에서 대기 환경을 조절할 수 있도록 하였으며, $N_2$와 $O_2$의 분율을 변화시켜 불렛 속도를 측정하였다. Intensified Charge-Coupled Device (ICCD) 카메라의 50 nsec의 노출 속도 조건에서 이미지 촬영을 통하여 불렛의 속도를 도출하였고, 발광분석법(Optical Emission Spectroscopy, OES)을 통해 제트의 위치에 따른 여기종과 이온화종의 정보를 얻고, 전기장을 계산하였다. 기존의

스트리머 이론의 모델에 근거하여, 전자 밀도와 유리관 내부 방전에 의한 전기장 효과를 반영하는 불렛 속도 모델을 제시하고, 실험결과와 함께 비교하였다. 불렛 속도는 주변 대기의 질소, 산소 가스의 혼합률에 상관없이 모두 세 개의 단계로 구분됨을 확인하였다. 첫 번째 단계는 가속 단계로, 외부에서 유입된 질소와 산소가 헬륨 준안정준위로 인해 페닝 이온화를 일으켜 전자 밀도를 증가시키고, 시간에 따라 불렛의 속도가 지수적으로 증가한다. 이 영역에서 음이온으로 인한 전자 손실은 전자–중성자 충돌 및 페닝 이온화에 의한 생성에 비해 무시가능하기 때문에, 주변의 산소 분율이 증가할수록, 불렛 속도가 증가하는 비율도 함께 증가한다. 두 번째 단계에서는 유리관 내부에 방전이 발생하고, 이로 인해 불렛의 진행에 반대되는 방향의 전기장이 발생하여 가속도가 감소하고 일정한 속도를 유지하며 진행한다. 이는 유리관 내 방전이 불렛의 처음 생성뿐 아니라 진행에서도 영향을 줄 수 있음을 나타내며, 연속적으로 변화하는 가스 조건에서 갑작스런 가속도의 변화를 설명해준다. 불렛이 진행할수록 제트 내부로 유입하는 산소의 분율은 증가하고, 헬륨 밀도가 감소하면서 불렛의 속도가 감소하는 세 번째 단계에 진입한다. 주변 대기의 산소 분율이 높을수록 두 번째 단계의 길이가 감소하고, 전체 제트의 길이 또한 감소한다.

불렛의 속도가 공기 중에서 세 단계의 분포를 가지고 있음은 불렛에 의해 생성된 전하와 라디칼 또한 공간 분포를 가지고 있다는 것을 나타낸다. 전하와 라디칼의 역할이 중요한 바이오 및 의학 분야의 적용을 위해서는 처리 목적에 부합하는 결과를 위하여 불렛 속도의 공간 특성을 고려한 처리 조건의 수립이 필요하다.

**제시어:** 헬륨 상압 플라즈마 제트, 불렛 속도, 속도 분포, 페닝 이온화